2016

Development of permanent magnet tubular linear motor and position feedback device based on Hall sensor

Songhan Pan
University of Wollongong

UNIVERSITY OF WOLLONGONG

School of Electrical, Computer and Telecommunication Engineering

Development of Permanent Magnet Tubular Linear Motor and Position Feedback Device based on Hall sensor

Songhan Pan

This thesis submitted in the fulfilment of the requirements for the

Award of the Degree of

Master of Philosophy

From the

University of Wollongong

March 2016

ABSTRACT

This thesis deals with the permanent magnet tubular linear motor (PMTLM) including the design and the manufacture. The motor is designed to have large output force with the limited height which could be used as the vehicle vibration reduction device in the future applications. There are many limitations of this tubular linear motor, for example, the length of motor, the cost of whole design and the considerable output force.

The electrical design and mechanical design are proposed in this paper. The Finite Element Analyse software Flux 2D is used in the project to model the permanent magnet tubular linear motor with a 2D axisymmetric boundary condition. In order to satisfy the limitations of the motor, all the simulations could be conducted by Flux 2D.

Moreover, the Hall sensor devices are applied to detect the position; as a result, the total cost of the system can be reduced a lot. At last, a tubular linear motor is built and the experiments about the motor and the feedback device are conducted.

ACKNOWLEDGEMENTS

There are many people who have supported me a lot during the way to completing my Master degree. I am very grateful for all they have done for me.

Firstly, I would sincerely like to thank my supervisors Asoc. Prof. Haiping Du and Dr. Philip Commins for their advices and encouragements. These advices and encouragements were absolutely invaluable throughout this project, not only for the technical aspect, but also motiving and encouraging me to move forward. I really appreciate the countless time they have spent to help me, such as teaching me the modelling technique by FEA software and providing me with the relevant information during the weekly meetings. I saved plenty of time and learned a lot of knowledge with their suggestions.

Also a huge thanks to Sean Ritchie from the workshop in University of Wollongong who spent many hours manufacturing and optimizing all the parts for my project.

I would also like to thank Shuai Sun and Donghong Ning who helped me to organize the servo hydraulic test system for the experiments of output force measurement.

Finally, I would like to thank my parents for all their supports and encourgingthroughout my university study.

TABLE OF CONTENTS

ABSTRACT i

ACKNOWLEDGEMENTS ii

TABLE OF CONTENTS iii

LIST OF FIGURES v

LIST OF TABLES vii

CHAPTER 1 Introduction 8

1.1 Introduction 8

1.2 Overview of Linear Motors 9

1.2.2 General Structure of Linear Motors 11

1.3 Aims and Objectives 13

1.4 Thesis Outline 14

CHAPTER 2 Literature review 15

2.1 Introduction 15

2.2 Position Detection Encoder 15

2.3 Tubular Linear Motor Design 17

2.4 Conclusion 19

CHAPTER 3 Mechanical and Electrical Design 20

3.1 Introduction 20

3.2 Development of PMTLM 20

3.2.1 PMs Tube Design 20

3.2.2 Armature Design 24

3.2.3 Simulation 28

3.3 Development of Linear Encoder Based on Hall-effect Sensors. 30

3.3.1 Introduction 30

3.3.2 Position Analysis 30

3.3.3 Mechanical Design of Linear Encoder by Hall Sensors 35

3.4 Electrical Design of Linear Encoder by Arduino. 36
3.4.1 Introduction 36
3.4.2 Model Design in Simulink 36
3.5 Conclusions 39
CHAPTER 4 Experimental testing 40
4.1 Introduction 40
4.2 Experiments of PMTLM. 40
4.3 Experimental Testing the Position Feedback Device. 42
4.4 Conclusions 43
CHAPTER 5 Results 44
5.1 Introduction 44
5.2 Force Generation 44
5.2.1 Simulated Force Output 44
5.2.2 Experimental Force Output 45
5.3 Hall Position Feedback Device 47
5.3.1 Magnetic Field Distribution in Simulation 47
5.3.2 Experimental Results 48
5.4 Conclusion 50
CHAPTER 6 CONCLUSIONS AND RECOMMENDATIONS 51
6.1 Summary 51
6.2 PMTLM 51
6.3 Position Feedback Device 51
6.4 Recommendations for Future Work 52
REFERENCES 53
APPENDIX A: Motor details 56
APPENDIX B: Simulatink model 67

LIST OF FIGURES

Figure 11: Photo of PMTLM. 9

Figure 12: The transition process from rotary motor to linear motor. 11

Figure 13: Four kinds of flat linear motors. 12

Figure 14: Different designs of PMTLMs. 13

Figure 31: Self-cantering steel pole shoe. 21

Figure 32: Segment of stator assembly. 22

Figure 33: Stainless steel tube with linear bearings. 23

Figure 34: Steel end cap. 24

Figure 35: Back cover with slot. 24

Figure 36: Coil container with one phase wound.[26] 25

Figure 37: Plastic container with coils. 26

Figure 38: Photo of PMTLM with rope encoder. 27

Figure 39: PMTLM model in FLUX 2D. 28

Figure 310: Isolines and isovalues of PMTLM. 29

Figure 311: Coil circuits in simulation. 29

Figure 312: Tubular linear motor topology. 30

Figure 313: Working principle diagram. 31

Figure 314: Distribution of magnetic lines. 33

Figure 315: Simulated magnetic flux density on X component. 34

Figure 316: Simulated magnetic flux density on Y component. 34

Figure 317: Specifications of Hall-effect sensor IC. 35

Figure 318: Fixture for Hall-effect sensors. 36

Figure 319: DAC module. 37

Figure 320: Calculation module. 37

Figure 321: Conversion module. 37

Figure 322: Parameters of the Coulomb & Viscous Friction Block. 38

Figure 41: Baldor driver system.[26]....40

Figure 42: Block diagram of Baldor driver and control system....41

Figure 43: Thrust measurement system....42

Figure 44: Block diagram of Hall sensor experiment....43

Figure 51: Simulated force output....45

Figure 52: Measured motor force as a function of applied current....46

Figure 53: Magnetic flux distribution....47

Figure 54: Harmonic analysis along X component....48

Figure 55: Harmonic analysis along Y component....48

Figure 56: Distribution of error markers (3mm)....49

Figure 57: Distribution of error markers (5mm)....49

Figure 58: Distribution of error markers (7mm)....50

Figure A1: Complete Assembly....55

LIST OF TABLES

Table 31: PMTLM electrical specifications. 26

Table 51: Measurement of force at different applied current. 45

CHAPTER 1 INTRODUCTION

1.1 Introduction

This thesis focuses on the design of a Permanent Magnet Tubular Linear Motor (PMTLM) and a position feedback device based on Hall-effect sensors. The work includes the design of the PMTLM structure and the exploration of the use of a position feedback device for the tubular linear motors. This thesis also includes software simulation and experimental results.

Many controlled objects must work in linear motion in a wide-range of applications. For example, in machinery manufacturing, aerospace industry, metallurgical industry and transport industry, there is strong desire for direct control methods instead of conventional rotary-to-linear solutions that include many mechanical conversion links such as a chain, steel wire rope, screw rod and worm gear. This sort of indirect solution has many disadvantages, and the varied conversion links, complicated configuration, and difficulty in design and manufacture restrict the overall efficiency of the system. The linear motor is a transmission system that changes electrical energy into linear motion mechanical energy without a buffering mechanism. Because of the various drawbacks posed by conventional rotary-to-linear counterparts, there is an increased interest in the direct drive mode based on linear motors, which possess simpler structure, higher efficiency, higher precision, lower response time, and lower noise.

Linear motor systems such as the flat linear motor and tubular linear motor have been widely used in industry applications, but much less attention has been paid to development of the Permanent Magnet Tubular Linear Motor (PMTLM). PMTLM has been used in high precision industry applications with a high cost of manufacture especially in the position feedback device. To ensure the linear hall sensor could be used with the position feedback device, the magnetic distribution must be sinusoidal, and a well-constructed PMTLM could meet this requirement. Economical PMTLMs for lower budget systems are being developed but there is much room for improvement. This thesis provides and tests an overall PMTLM design which includes the simulation of a motor using the Finite Element Analysis software Flux 2D. The optimization of a position feedback device is also proposed and both

simulated and experimentally verified. The PMTLM was designed and shown in Figure 1.1.

Figure 11: Photo of PMTLM.

1.2 Overview of Linear Motors

1.2.1.1 History of Development

The development of linear motors can be traced back to 1840 when Wheatstone proposed and designed an unsuccessful linear motor [1, 2]. In the 175 years since that initial experiment, the development of linear motors can be considered in three periods from the early experimentation to a stage of improved utilization and to a time of commercialization [3].

(1) First stage (1840-1955)

Linear motors developed from the imagination to the experimentation stage with little success. A first patent for using the linear motor in looms was published in 1895 and in 1905, a description of using a linear motor as the actuating unit for a train was published [3, 4]. However, both of these ideas remained in the early experimental

demonstration stage. In 1917, the first tubular linear motor was designed and people tried to develop it for use in a missile launcher, but this project never made it passing the experimental stage [3]. From 1940 to 1955, the first experimental applications of linear motors made it to the manufacturing stage. In 1945, the Westinghouse Electric manufactured the first electric traction aircraft catapult in USA and in 1954, the Royal Aircraft Establishment in UK produced a missile launcher using a double-sided flat linear motor, which allowed speeds up to 1600km/h [2].

However, at this stage, the linear motor saw limited application as it was unable to compete with the rotary motor in terms of cost and efficiency. Therefore, the linear motor was not extensively developed at this time.

(2) Second Stage (1956-1970)

Starting in the 1950s, owing to the development of control technology and years of experimental theory, the linear motor has entered a new stage of comprehensive development [5]. During this period, Professor Laithwaite published a fairly comprehensive monograph “Induction Machines for Special Purpose”, which stimulated interest and made a significant contribution to the field of linear motors [2]. After 1965, more and more equipment based on a linear motor was developed, such as the electric gramophone, sewing machine and conveyer device [3].

(3) Third Stage (1971-current day)

In this period, linear motors entered the commercialization era. Many varieties of linear motors appeared world-wide, not only in industry areas, but also in people’s daily life. The first commercial operating magnetic-levitating train was launched in China capable of a maximum speed of 500km/h [5]. The linear motor was also developed and widely used in tools such as an automatic graph plotter, scanner recorder, and linear potentiometer [6].

At this point, linear motors are in a stage of ongoing development, using processes that allow these motors to compete with the rotary motors but they also have particular advantages [5].

1.2.2 General Structure of Linear Motors

The linear motor can be described in relation to the original electric rotary motors as a rotary motor split in the radial direction and then unfolded in a straight line as shown in Figure 1.2 [7]. In the linear motor, the stator and rotor are 'unrolled' so that the motor produces a linear force along its length instead of by producing a torque or rotation as the rotary motor does [8-10]. As a result, the stator and rotor parts in the rotary motor become the primary and secondary sections, respectively, in the linear motor. However, the rotor can be either within the primary section or secondary section in different structures of linear motors.

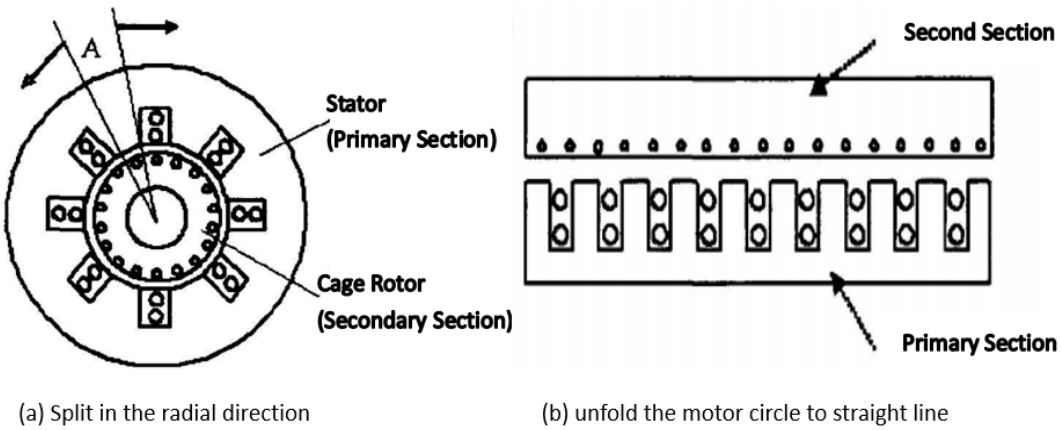

Figure 12: The transition process from rotary motor to linear motor [7].

There are four different varieties of linear motors that differ in their fundamental structure: flat, tubular, disc-type and arc-type. The disc-type and arc-type are similar to rotary motors as they still rely on rotary motion [11]. Here, the structures of the flat and tubular linear motors are discussed.

The flat linear motors shown in Figure 1.3 are classified into four kinds based on the structure of being either single or double sided and depending on the length of the primary and secondary sections [12]. All of these flat linear motor variations can be used in different applications.

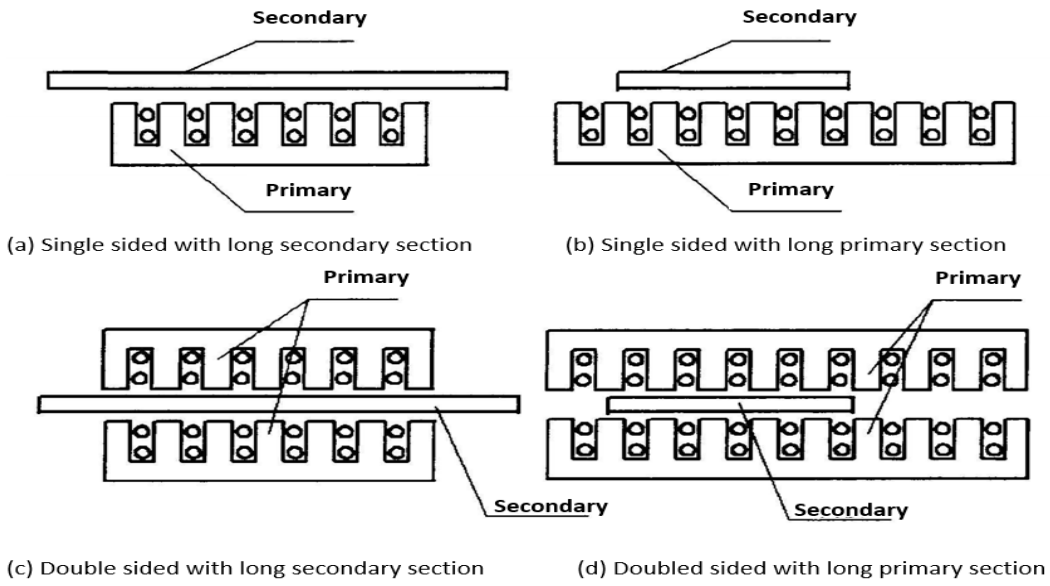

Figure 13: Four kinds of flat linear motors [12].

In addition to these flat linear motors, the tubular linear motor is another main category of linear motors. The Permanent Magnet Tubular Linear Motor is a kind of the tubular linear motor which has a simple structure, zero net attractive force, no end windings, and a high thrust to weight ratio [13, 14]. Another advantage of PMTLMs over the flat linear motors is their structural similarity to the conventional rotary-to-linear counterparts, which facilitate their upgrade and replacement in applications. The permanent magnets in PMTLM have been designed in three different ways [9, 15, 16] as shown in Figure 1.4: radially magnetized surface mounted PMs, axially magnetized buried PMs, or both radially and axially magnetized, as in a Halbach array [14].

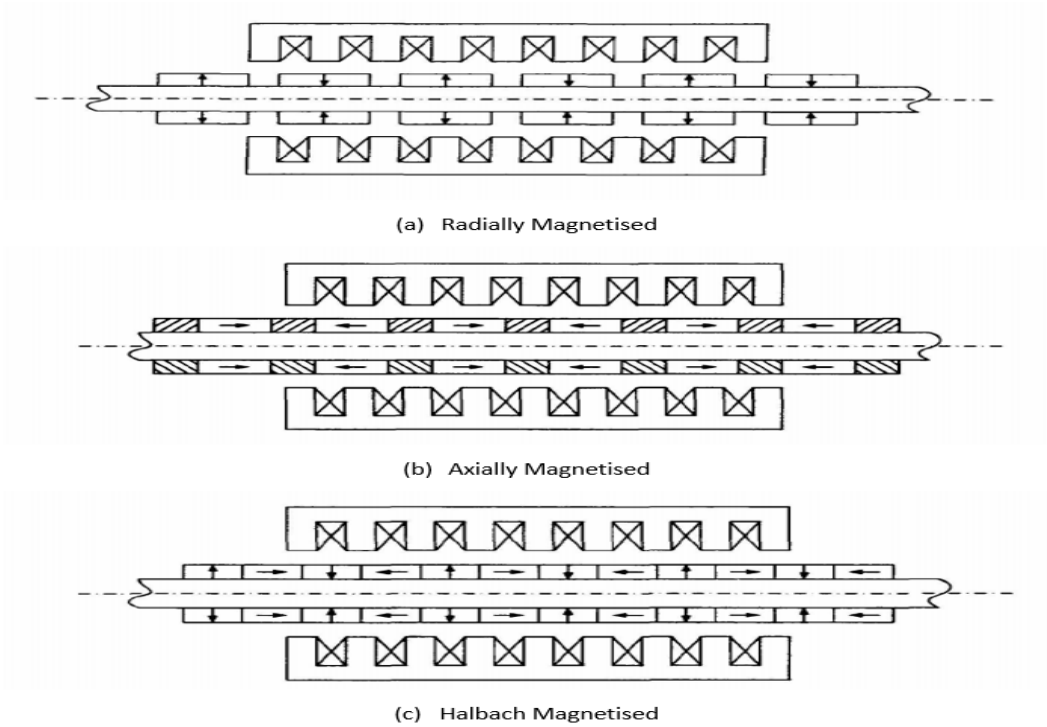

Figure 14: Different designs of PMTLMs [17].

1.3 Aims and Objectives

The aim of this thesis is to develop an effective and economical Permanent Magnet Tubular Linear Motor (PMTLM). A PMTLM has been designed and tested using a standard servo driver and associated equipment. The simulation of design was conducted using Finite Element Analysis (FEA) software Flux 2D, and the Hall sensor encoder used the Arduino Board and was programmed by Simulink

The objectives for the research:

- Computationally design the motor model and obtain simulation results.
- Design a position feedback device based on a Hall sensor.
- Manufacture the PMTLM and the linear position feedback encoder.
- Develop control system of position feedback device by Arduino board.
- Test the PMTLM with the servo driver.

The position feedback device plays an important role in the linear motor system, thus, this thesis included the design of the linear motor and the design of a Hall position feedback device. The combined system could be used for applications which require high thrust with low cost, such as an active vehicle suspension system.

1.4 Thesis Outline

Chapter 1 introduces the work in this thesis and outlines the contributions of each chapter. The history of the development of PMTLM is described and the different types of linear motors are presented. The aims, objectives, and structure of the thesis are presented.

Chapter 2 presents a review of background literature. The chapter is divided into two sections focusing on the design of PMTLM and the development of position feedback devices based on Hall sensors.

Chapter 3 details the PMTLM and Hall sensor feedback device developed here. The mechanical and the electrical design for PMTLM and Hall sensor feedback device are introduced. The Arduino board is employed as the microcontroller.

Chapter 4 discusses the experimental tests of both the PMTLM and Hall sensor position feedback device. Details of the completed experimental equipment are presented.

Chapter 5 is an analysis of data from both the experiments in Chapter 4 and the simulation in Chapter 3. By comparing the data, the force constant of PMTLM and the ideal position for Hall sensors can be determined. Suggestions for further work in this area are also identified.

CHAPTER 2 LITERATURE REVIEW

2.1 Introduction

This chapter describes the modelling of the PMTLM, with general analysis of PMTLM and the position feedback technique. The previous research on slotless PMTLM is presented in this chapter, with respect to the structure optimization and motor design. Special attention to structure optimization is a key concern for PMTLMs, where it has been shown that the precision of position feedback device based on linear Hall sensors can be greatly increased with optimal geometry. The findings reported here confirm that optimized geometry allows improved precision by generation of a better sinusoidal magnetic field distribution.

The chapter also discusses the utilization of Arduino platform. In the linear motor feedback device based on linear hall sensors, the Arduino board is used as the processor.

2.2 Position Detection Encoder

An accurate position of the moving part is critical for linear motor control, regardless of the control scheme details [18]. This position detection is one of the most crucial components of the whole servo control system that directly affects the precision of motor control and operating performance. Currently, the linear optical encoder is the most commonly used feedback device in high precision servo systems [19].

C.Chen and M.Cheng [20] describe a cost-effective position control system for an ironless linear motor. They picked the specific sensors to regulate the space current vector instead of using more costly position or current sensors. While the authors discuss the results with and without dead time, a strategy to eliminate the position error caused by missing steps was not discussed and there was no proposal for how to reduce the influence of switching dead time. Although the experimental motor they used in this paper is a flat linear motor, this kind of position detection theory could be used in other systems.

In [21], Liu et al. present a slotless TLM with buried PMs, and they use a simple and inexpensive Hall Effect sensor unit to measure the magnetic field distribution along

the magnet tubular. Using data from two sensors were mounted to one side near the edge, the magnetic field was measured and the authors discuss the influence of the backiron. Based on this study, the electrical angle difference of the two sensors is 90 degrees, and the output and can be indicated as:

(2.1)

(2.2)

(2.3)

where is the electrical angle in Hall sensor "a" and is the maximum output from Hall sensor. However, experimental results show an average error of 0.6mm compared to the current linear optical encoder with 0.05μm accuracy [21].

Paul and Chang [22] proposed a new mover position detection method using the same sensor as in [21]. They compared the three-phase method with the conventional two-phase method which used two sensors. Their results were verified through Matlab and experiments and suggest that the three-phase method could improve measurement accuracy. The algorithm used in this paper is as follows:

; ; (2.4)

The three to two phase transformation results in:

(2.5)

(2.6)

Based on the findings in these two papers, a position detection device using hall sensor is feasible and suitable to some low cost actuators due to the non-negligible cost of optical encoder [21]. Even though the accuracy and response speed require further research, the Hall Effect sensors have emerged as a popular alternative to conventional optical encoders. PMTLMs are now available from Copley Controls Corp. [23] that are assembled with linear encoder based on Hall sensors with a claimed accuracy of 400 μm.

In [21], the authors also discussed the mounting position of Hall sensors. Designs were compared where the first hall sensor was positioned 2mm, 10mm, 15mm, or 18mm away from the armature. The results showed that at 2mm, the max error is 9.4mm and this error decreased when the sensor was positioned at 15mm and 18mm. This work focused on the position in the axial direction, but the optimal position in radial direction still requires further study. Study of the magnetic flux distribution of tubular linear motors [24] found that the closer the Hall sensor is to the permanent magnets, the more flux will go through the Hall sensor but the proximity also causes a larger flux aberrance. Therefore, an appropriate position should be determined to ensure obtaining a sufficiently large output and optimally detecting a sinusoidal magnetic field.

2.3 Tubular Linear Motor Design

Many different types of Permanent Magnet Tubular Linear Motors are currently in use. For example, Xu, et al. [25] designed a tubular linear permanent magnet synchronous motor to replace the normal beam balanced pump system which is used in oil-wells to increase efficiency and decrease the occupied ground space. Li and Zhang [26] proposed a new actuator for cryocoolers based on a PMTLM with Halbach magnetization. They built two motors and compared them for efficiency and power. However, the two tested motors were just geometric variants of general PMTLM and the cost of the position detection devices were not explicitly considered.

As mentioned in 2.2, the position detection device obtains position feedback by measuring the magnetic field through Hall-effect sensors. It is necessary to design the magnet tubular stator with an appropriate magnetic flux distribution so that the linear hall sensor can get accurate input. In order to get a better sinusoidal magnetic field distribution, a widely used strategy to optimize flux distribution uses an appropriate ratio of magnet length and pole pitch [9, 27]. Wang et al. found that when the ratio of magnet length and pole pitch was changed from 0.4 to 0.9, the force density increased. Meanwhile, at a ratio of 0.66, the magnetic field distribution could become sinusoidal. Although not mentioned in the paper, a ratio of magnet length and pole pitch of 2:1 could provide a better flux density distribution [9, 27].

The tubular linear motor is expected to be run smoothly but there can be an influence of cogging force [11, 28, 29]. The cogging consists of two components, the armature end effect and the tooth ripple. Atencia et al. [30] presented a solution for cogging reduction by optimizing the size of the iron core and adding it to the slotted armature to decrease the influence of the armature end effect. The optimal length of magnet reduced the effect of tooth [31]. This report showed an excellent reduction of cogging by these two improvements. Ohto et al. [32] described another way to reduce cogging by optimizing the end teeth. In order to reduce the tooth ripple cogging, the armature was stretched by one pole pitch. Different from the normal skewing, the magnets remain parallel to each other. Both studies [30, 32] used a similar approach to vary the end of armature and reduce cogging. Even though skewing the magnets is a simple way to reduce cogging, this reduces the minimal force output.

It is full of significance to describe the motor features with an appropriate and accurate model so that precise simulation and predictions can be obtained fast [33]. Two widely used motor analysis methods are mathematical analytical methods and numerical approximation using FEA method.

Wang, et al.[34] provide a generous framework to describe the magnetic field distribution in a PMTLM using analytical method. The study deals with the magnetic flux distribution, the flux linkage, and the analysis of cogging force. While no experimental validation was given and the effects of the finite length stator were not particularly considered.

In recent years, FEA method has been widely used to model electrical motors [35, 36]. For tubular linear motors, 2D axisymmetric boundary conditions are continually encountered [37-39]. The FEA method takes into account the non-linearity features such as material saturation, winding construction, flux leakage and the complex geometry of the system with considerable accuracy results [17]. The fast and accuracy results depend on the mesh size, while a rough mesh size might be suitable for the general flux calculation, a fine mesh is necessary for the high accuracy force analyse [40]. In the later project, the FEA software Flux 2D was used to model the tubular linear motor.

2.4 Conclusion

The literature review illustrated that methods for position detection based on Hall sensors have been developed for PMTLMs, but there are several different theories and a linear encoder based on Hall sensors has not been studied significantly. The mounted position of Hall sensors have been studied, and the appropriate position for the sensors could improve precision and decrease the influence of end magnetic field distortion.

This chapter also discussed the geometry of PMTLMs, the two components of cogging force, and how the cogging force could be reduced by effective design. The ratio of magnet length and pole pitch is important to generate a sinusoidal magnetic field along the tubular stator.

CHAPTER 3 MECHANICAL AND ELECTRICAL DESIGN

3.1 Introduction

This chapter discusses the design of the PMTLM. Computer Aided Design software was used to design all the parts of PMTLM prior to construction. The details of the stator dimensions and the construction of armature are described and the assembled model is presented.

Next, a brief description of the mounting position of Hall sensors is presented. The mounting position was selected after evaluation of the magnetic field distribution to identify the ideal position. The radial position of Hall sensors can be altered to provide a better sinusoidal magnetic field.

Finally, the Simulink program for the Arduino board used as the microcontroller is described. Voltage is the output from the Hall-effect sensors and the microcontroller performs the calculation to obtain the position. This position data then transferred to the square waves that are read by the servo driver directly.

3.2 Development of PMTLM

3.2.1 PMs Tube Design

There are several aspects of motor design that are limited by market availability, such as the cylindrical magnets and seamless stainless steel tube. It was important to assess what parts requiring manufacturing and what parts could be purchased as standard parts. It was necessary to determine the source of the components before any simulations were conducted.

In PM motors, the stator may be the most confined component due to limited available materials. The design of permanent magnets and seamless stainless steel tube must take market supply into account. The processing of this component prohibited modification of the length of the inside diameter and only the outside surface of stainless steel tube could be machined to size. Based on this, we used the existing inside diameter of the tube and designed the diameter of the permanent

magnets to match as closely as possible, to not allow extra movement between the magnets and tube when the motor is working.

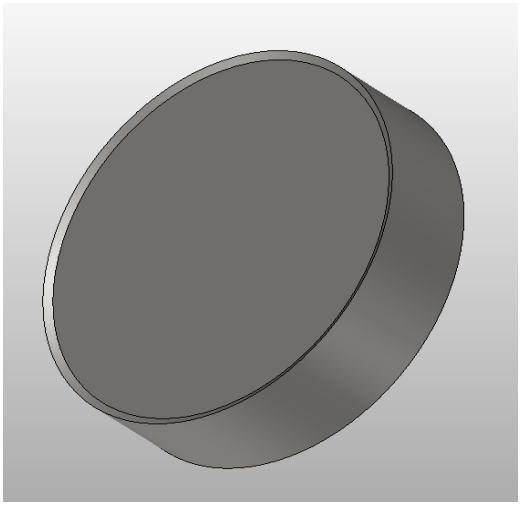

Figure 31: Self-cantering steel pole shoe.

Cylindrical magnets 40mm in diameter and 20mm in length were selected based on market availability. A seamless stainless steel tube was chosen from a local company with an inside diameter 1mm larger than the magnet diameter. The steel poles were designed to position the permanent magnets and hold them in the tube tightly. As shown in Figure 3.1, the steel poles were designed with an extra border to fit the rounded edge of the magnets and maintain the magnets in the centre. The full dimensions are given in Appendix A. When the magnets and steel poles are put together, they were joined firmly in the centre with the help of this extra border as shown in Figure 3.2.

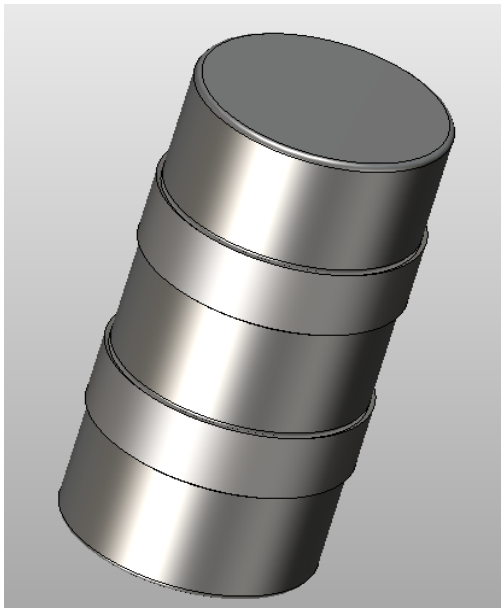

Figure 32: Segment of stator assembly.

The chosen stainless steel tube was seamless, schedule 40, grade 316. This grade of product shows high strength and low magnetic permeability. The tube houses the permanent magnets and steel poles. The wall thickness should be as thin as possible to allow air permeability so that there is no effect to shield the magnetic flux. Given the market availability, a stainless tube of inside diameter 41mm and 3.683mm wall thickness was chosen. The length of tube was machined to 310mm, long enough to hold 20 magnets and 11 pole pieces. The entire stator has 11 similar pole pitches.

Each pole pitch is made up of a 20mm length magnet and a 10mm length steel pole shoe for a length of 30mm in total. The detailed drawings and complete dimensions of all the components are presented in Appendix A.

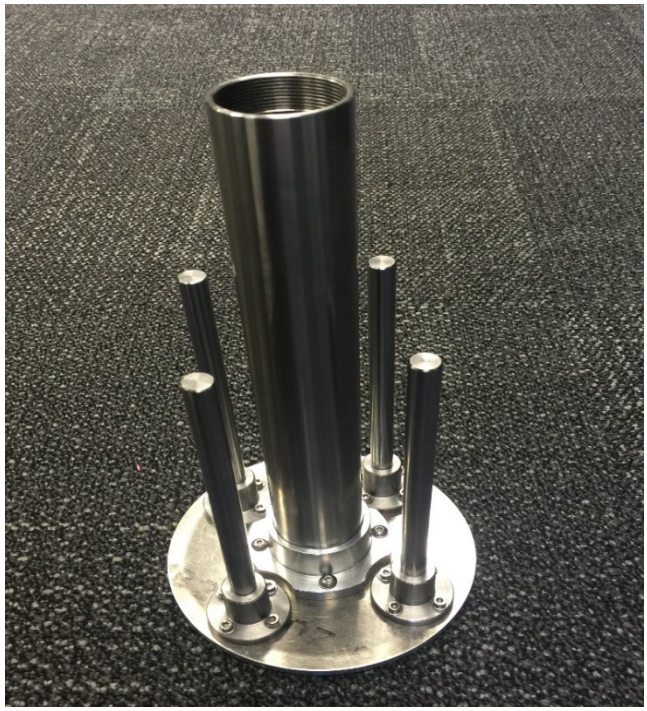

Figure 33: Stainless steel tube with linear bearings.

As described in 2.3, the force density increased when the ratio between the length of magnets and pole pitch was varied from 0.4 to 0.9 and the force ripple showed a minimum when the ratio was around 0.7. Given these parameters and taking both performance and magnet cost into account, a ratio of 0.66 was picked so the magnet length of 20mm and entire pole pitch length of 30mm was chosen for a ratio of 0.66.

A photo of the machined stainless steel tube is shown in Figure 3.3, after being mounted with the upper plate and four linear bearings. The magnets were placed in opposition, North pole against North pole and South pole against South pole with a steel pole shoe in the middle. The magnets were inserted by a slim stick and assembled together by the steel pole shoes without any external force. When the magnets were inserted into the tube, there was an initial repelling force due to the opposition. However, once the magnets touched the poles, the resultant attraction force was generated and held the assembly together. Finally, a steel cap as shown in Figure 3.4 was attached to the end to ensure all the magnets and pole shoes were fixed firmly in the tube; this cap also serves as the last pole shoe in the assembly.

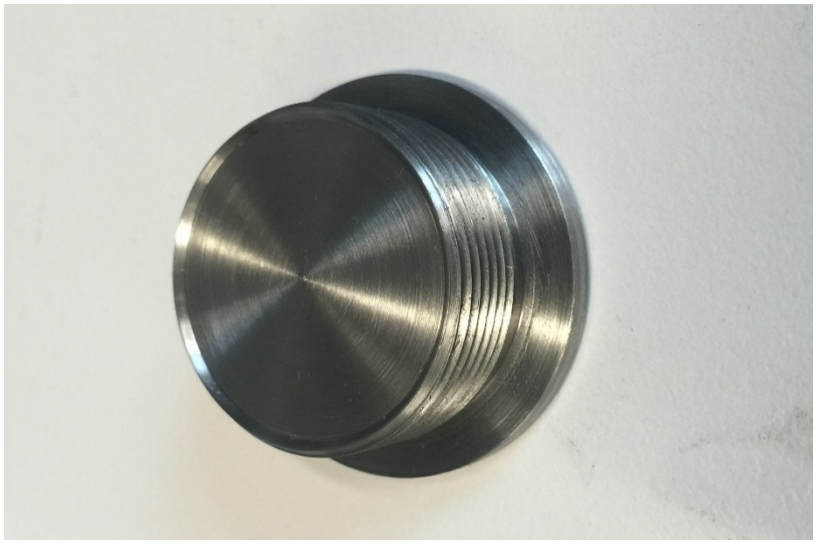

Figure 34: Steel end cap.

3.2.2 Armature Design

The slotless armature was composed by the coils and back cover. It is a relatively straight-forward design with a back cover housing the coils in the middle.

As shown in Figure 3.5, a cut was placed in the back cover to allow the wires to exit the back cover for connection. The inside edge was rounded off to provide sufficient room to minimize contacts of wires and short circuits.

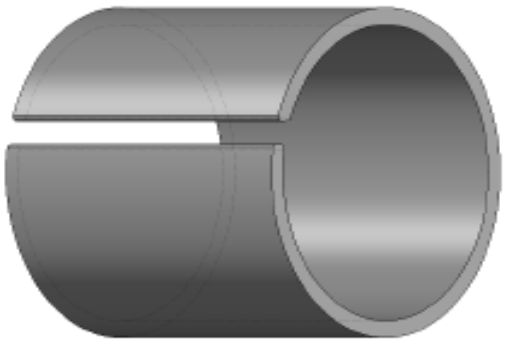

Figure 35: Back cover with slot.

A plastic container was used for the coils. As shown in Figure 3.6, the whole container was divided into 12 slots and a thin wall separated each slot. Three radial cuts in the wall were located 120 apart from each other to maintain the strength of the walls. These cuts allow a single wire to be used to connect one coil to its partner coil,

crossing two other coils. The two partner coils were made from a continuous strand to minimize the connection problems and insulation paper was used on the crossing wire.

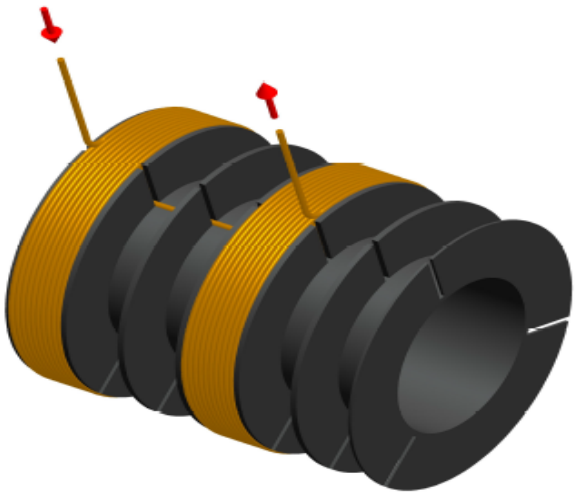

Figure 36: Coil container with one phase wound. [24]

Each phase of coils was wound in the same direction at the same time, which was a simple way to achieve the correct orientation with the desired winding structure. As shown in Figure 3.6, the current enters the left coil, flows clockwise around the coil, and then travels to the right coil in a counter-clockwise flow. This kind of winding allows simple, stable, and fast construction. For mass production, winding of all the coils at the same time would be recommended to reduce manufacturing time. Once all the coils were wound, the surface of the coils was wrapped with a layer of insulation paper and then the back cover was closed tightly.

Only one strand per coil should protrude from the coils as all the connecting strands between phases run underneath the coils. The container fixes the coils in position tightly to minimize rubbing against the stator in case of any misalignment. It is important to fill as much of the container as possible. For this reason, the wall of the container should be as thin as possible. In consideration of running heat the plastic of the container should be hard and resistant to high temperatures.

As can be seen in Figure 3.7, the coils were wound such that each coil has 110 tums of 0.8mm diameter wire and each coil was in the desired orientation. The surface of

each coil was covered with silicon and then wrapped with insulation paper to prevent short circuiting.

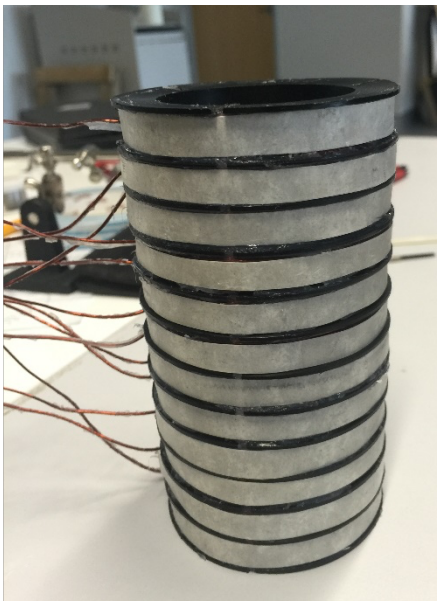

Figure 37: Plastic container with coils.

The armature consists of 12 coils in three phases covering 4 pole pitches. Two round aluminium plates hold the armature with four stainless steel threaded rods at each corner. Another aluminium tube was in the bottom to hold the armature up and provide the space for the stator. A 2mm slot was manufactured in this aluminium holder to eliminate the electromagnetic force that results when the permanent magnets stator passes the aluminium tube.

The electrical specifications of the built motor are outlined in Table 3.1.

Table 31: PMTLM electrical specifications.

Specification	Value	Unit
Number of turns (per coil)	110	
Number of coils per phase	4	
Number of turns per phase in series	440	
Resistance (phase)	8.62	Ω
Inductance (phase)	9.15	mH
Maximum working voltage	300	V
Rated current	3	A
Continuous stall current	3	A
Peak current for 1 second	12	A
Current Density at 1 A	1.36	
Maximum coil temperature	80	°C

A photo of the complete motor construction showing the stator and armature mounted together and the linear bearing is shown in Figure 3.8. The armature was fixed by two nonmagnetic aluminium plates with 4 stainless steel threaded rods. The linear bearing was used to restrict the rotary movement between the armature and stator. A rope linear encoder was used for position feedback and compared with the Hall sensor linear encoder. The drawings in Appendix A show the details of all the parts of this motor.

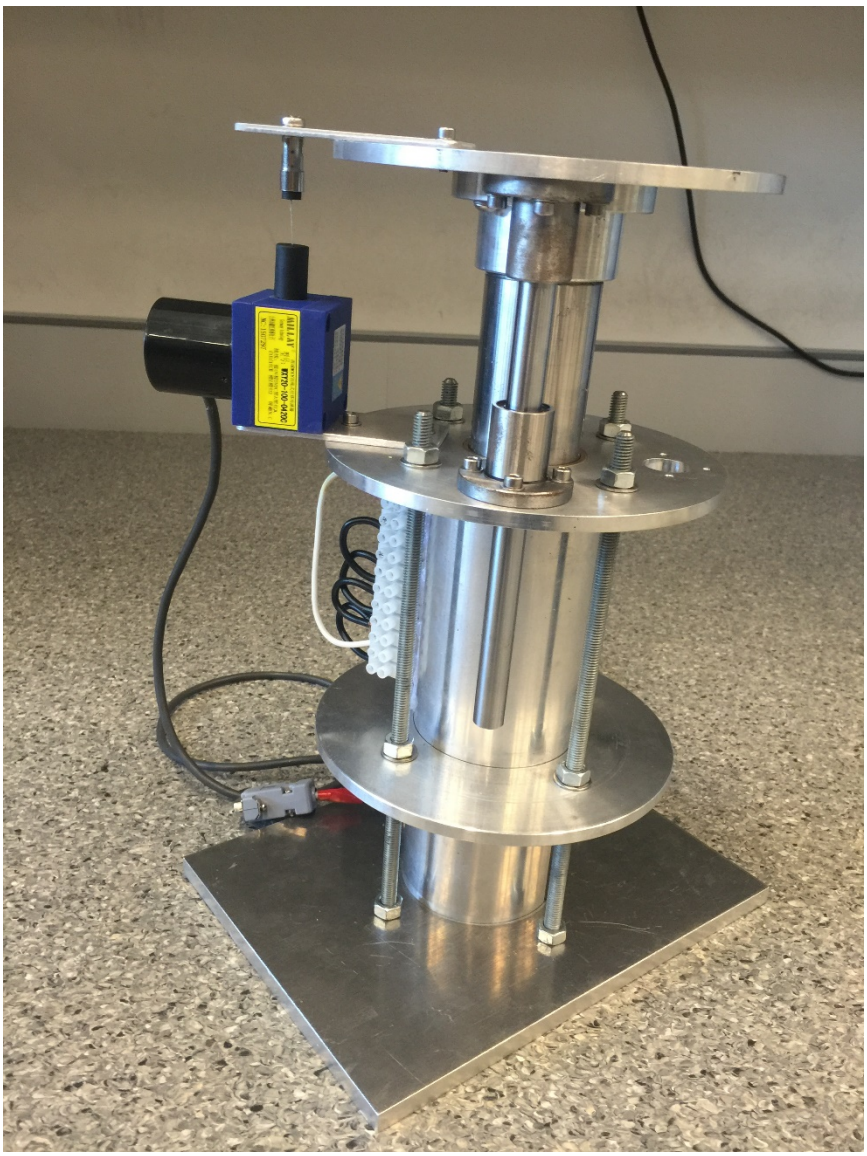

Figure 38: Photo of PMTLM with rope encoder.

3.2.3 Simulation

It is imperative to describe the motor characteristics with an appropriate and accurate model to get accurate simulations and predictions when the parameters change. Unlike conventional mathematical analytical methods, the FEA software enables rapid acquisition of results from simulations. In this study, the FEA software Flux 2D developed by CEDRAT was used to get the simulation results.

Because the linear motor has axial symmetry, the simulation model was simplified to 2D in the FEA software. Based on the actual size of magnets and stainless steel tube, the model of PMTLM was built as shown in Figure 3.9.

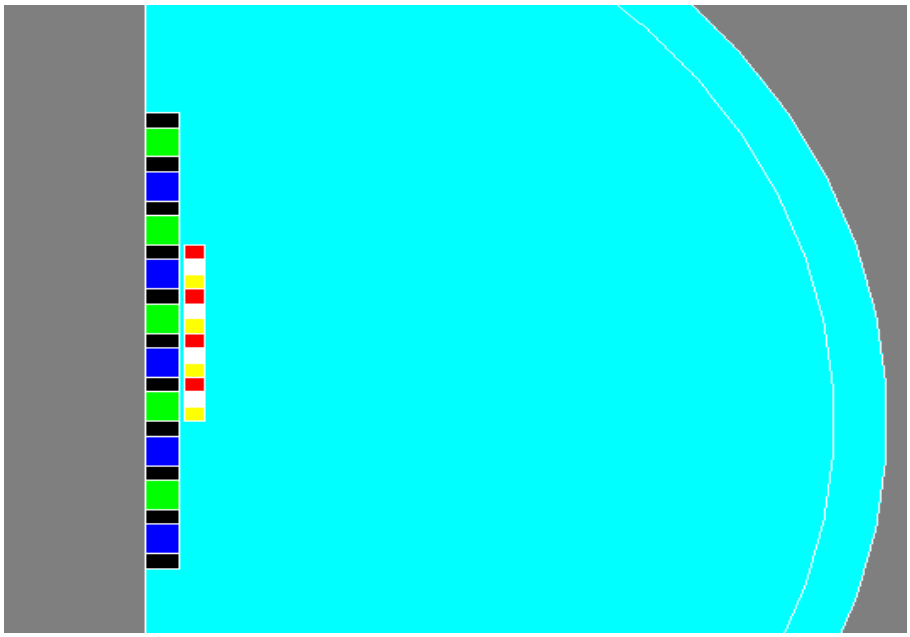

Figure 39: PMTLM model in FLUX 2D.

The blue and green represent the two opposite magnets, the black part is the steel pole shoe, and the coils in three different phases are shown in red, white, and yellow, respectively, and the turquoise part is the infinite air area. The distribution of the magnetic field isolines and the flux isovalues were acquired in Flux 2D as shown in Figure 3.10.

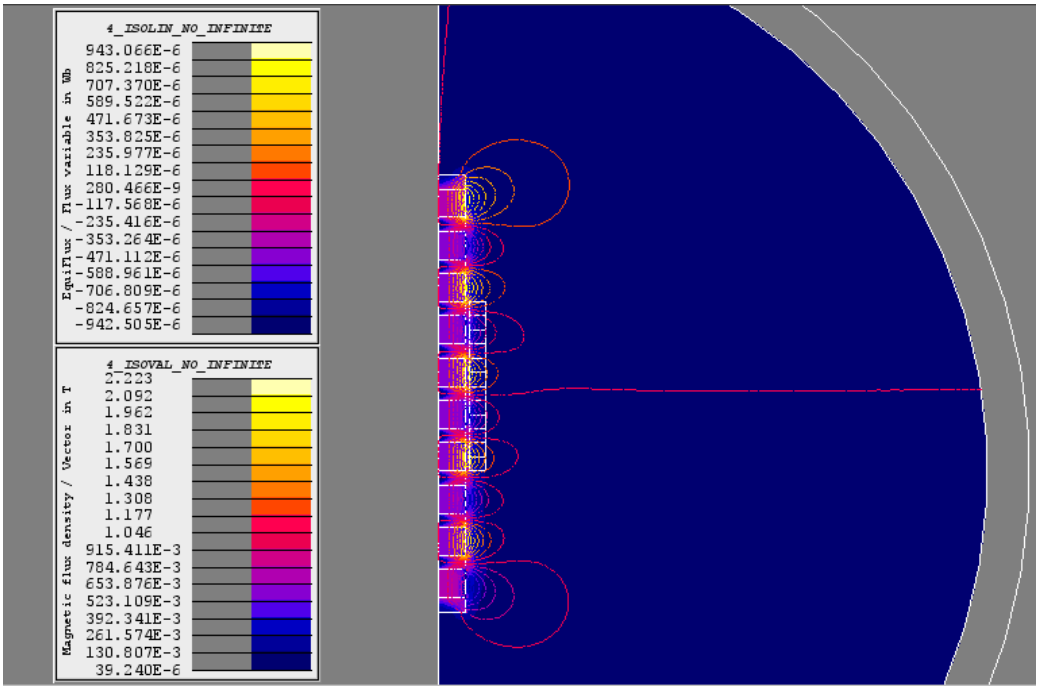

Figure 310: Isolines and isovalues of PMTLM.

The circuit of coils can be set in the software and Figure 3.11 shows the winding orientations. The winding orientation was designed according to a standard 3-phase system. The model is divided into two parts, the stator and the armature, the mechanical set of the stator is fixed and the armature is moving.

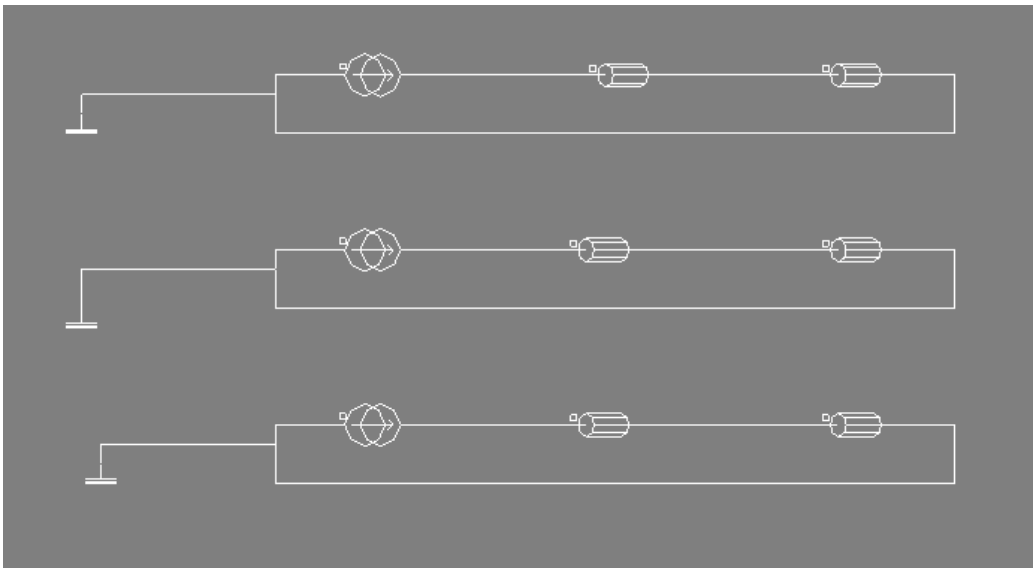

Figure 311: Coil circuits in simulation.

3.3 Development of Linear Encoder Based on Hall-effect Sensors.

3.3.1 Introduction

A linear Hall sensor can be used to detect magnetic flux density within a magnetic field. The voltage output from the Hall sensor generally exhibits a linear relationship to the measured magnetic flux density. The position of the moving part can be determined by detection of the magnetic flux density due to the sinusoidal distribution of magnetic field in a PMTLM air-gap. This section demonstrates this approach with the PMTLM.

3.3.2 Position Analysis

As shown in Figure 3.12, the Hall sensor is mounted on the edge of the moving part above the permanent magnets to measure the position of the moving part as it moves on the X axis. A previous study [36] showed that the magnetic flux density (B) in an air-gap follows a sinusoidal distribution. As a result, at least two linear Hall sensors are required to measure the position of the stator. Appropriate mounting of the sensors requires: (1) The two Hall-effect sensors should be horizontal on the X-axis. (2) The distance between two Hall-effect sensors should be half a pole pitch on the X-axis.

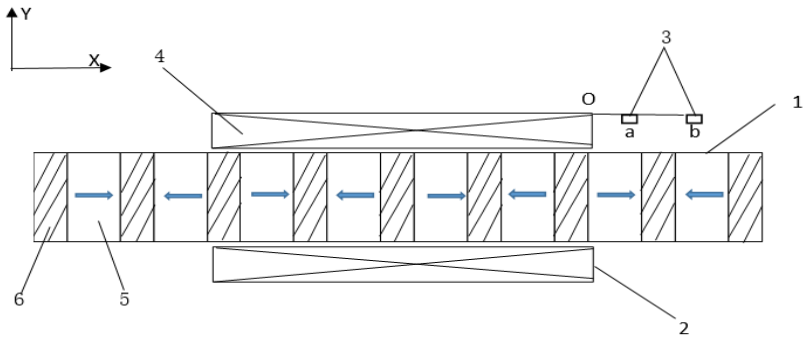

1. Stator; 2. Armature; 3. Hall-effect sensors; 4. Armature windings; 5. Permanent magnets; 6. Steel pole shoes.

Figure 312: Tubular linear motor topology.

The basic principle is illustrated in Figure 3.12. When the moving part moves along one pole pitch, the sinusoidal flux distribution in the air-gap along the X axis would cause the resulting voltage output from the linear Hall-effect sensor to also be

sinusoidal. So the pattern shown in Figure 3.13 can be regarded as the combined flux distribution curve and the voltage output curve from the Hall-effect sensor. There is no magnetic flux passing through point O in Figure 3.13 at the start of the experiment. The distance from 'O' to 'a' and 'b' is and respectively, and and follow the equation =+/2, where is the pole pitch. Because the electrical angle difference of the two sensors is 90 degrees, the output and can be written as:

(3.1)

(3.2)

where is the electrical angle in Hall sensor "a" and is the maximum output from the Hall sensor.

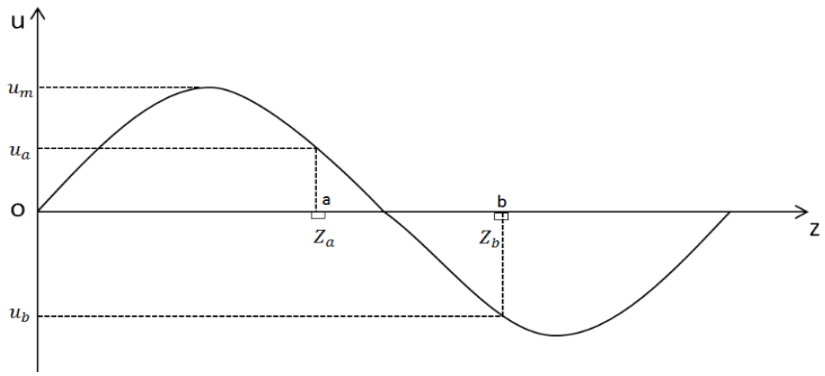

Figure 313: Working principle diagram.

Based on and , the electrical angle in the position of Hall "a" can be determined easily. Generally, there are two algorithms used for two or three linear Hall-effect sensors to calculate the position.

1) Algorithm for using two Hall sensors.

Use the voltage outputs from two Hall sensors to calculate the electrical angle:

(3.3)

2) Algorithm for using three Hall sensors.

Use the output from three Hall sensors outputs to calculate the electrical angle:

; ; (3.4)

The three to two phase transformation results in:

(3.5)

(3.6)

In comparison with using two Hall sensors, the solution of using three Hall sensors detected the magnetic flux in three positions, so three voltage outputs were transferred into and which are equivalent to and , respectively, in the solution using two Hall sensors. The core theories used for these two methods are the same; however, the precision is increased by the use of three Hall sensors.

Along one pole pitch, the position of the motor depends on the measured flux density by mounting Hall sensors in "a" and "b" along the X-axis. As a result, the measurement has two errors, a mounting error that can result from an inaccurate mounting position as described above and magnetic flux aberrance. In this section, we mainly focus on the magnetic flux aberrance.

Owing to the lack of continuity and the finite length of the armature, the edge effect affects the magnetic flux distribution near the edge of the armature causing the Hall sensor output to deviate from the standard sinusoidal signal. To eliminate this aberrance, the flux density should be analyzed to find an ideal position for mounting the Hall sensor.

Figure 3.14 shows the distribution of magnetic flux lines in the coils area.

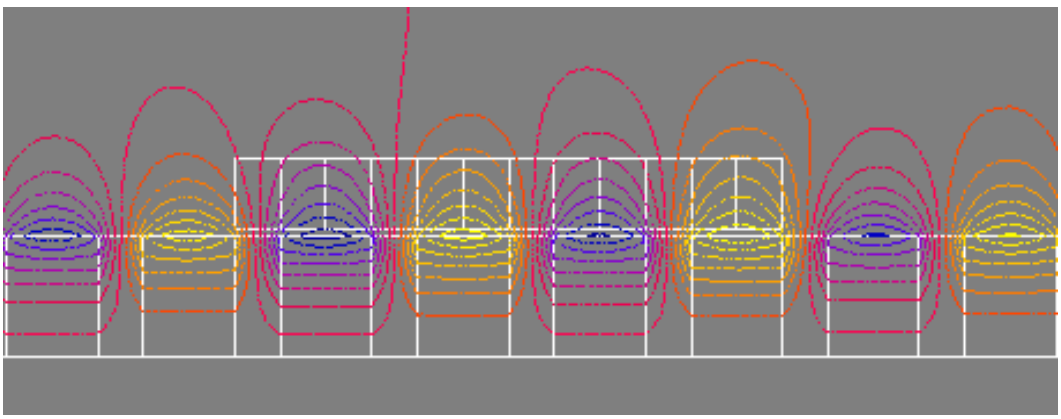

Figure 314: Distribution of magnetic lines.

L. Xiao [21] proposed that the Hall sensor position should be a certain distance away from the edge of the secondary windings to avoid it being affected by magnetic aberrance. Here, we focus on optimal placement of the mounting position in the radial direction (Y-component). Study of the magnetic flux distribution of tubular linear motors [36] suggested that the closer the Hall sensor is to the permanent magnets, the more flux will go through the Hall sensor, but this proximity also causes a larger flux aberrance. Therefore, selection of an appropriate position must allow sufficient output and detection of a sinusoidal magnetic field.

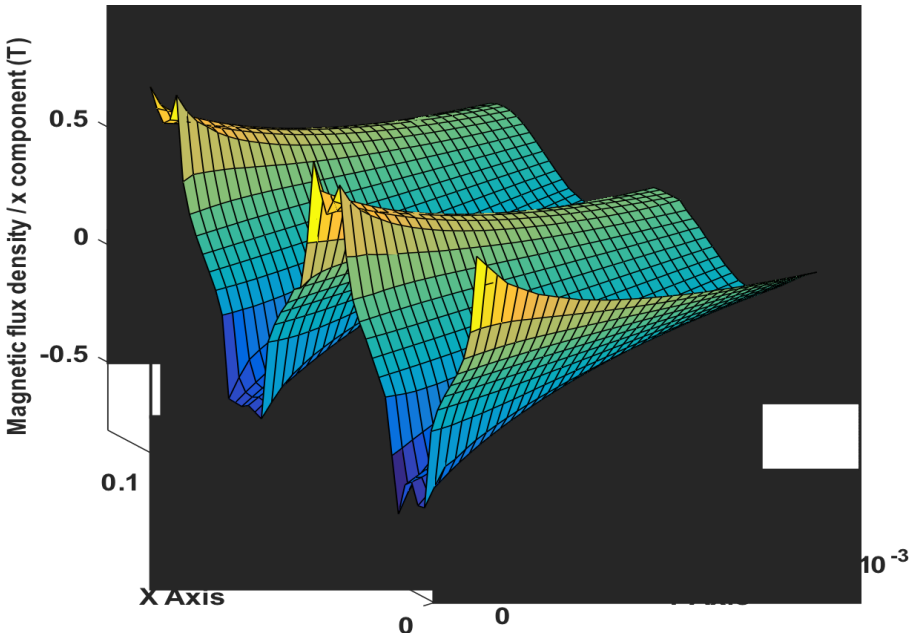

Figure 315: Simulated magnetic flux density on X component.

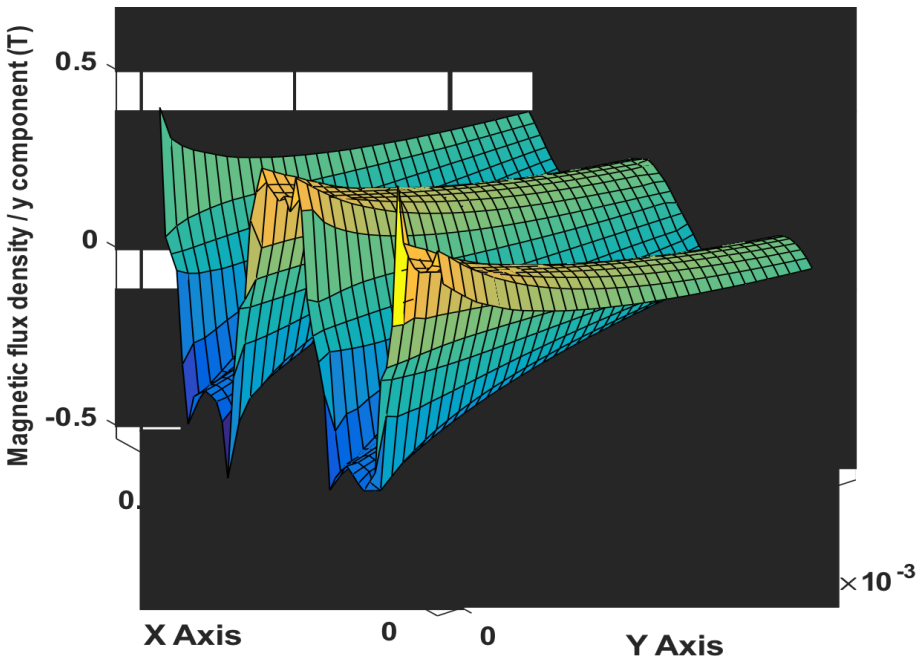

Figure 316: Simulated magnetic flux density on Y component.

As shown in Figures 3.15-3.16, we can use Flux 2D software to determine the flux distribution on X and Y components.

3.3.3 Mechanical Design of Linear Encoder by Hall Sensors

The Linear Hall-effect Sensor IC, Honeywell product SS49E, has the specifications indicated in Figure 3.17. These Hall-effect sensor ICs are small, transducers that vary their output voltage in response to a magnetic field from a permanent magnet or an electromagnet. They are designed and manufactured for cost competitiveness as system components.

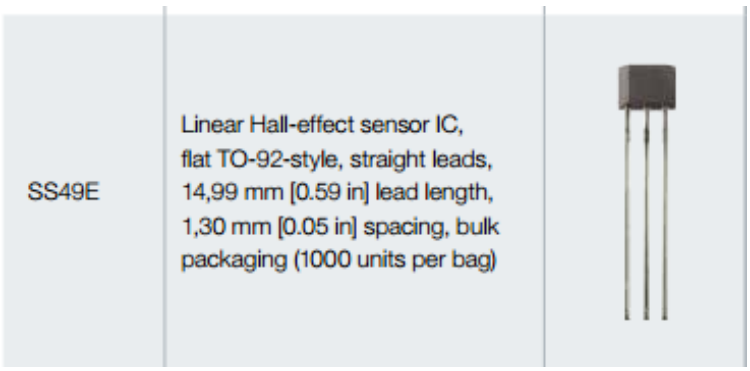

Figure 317: Specifications of Hall-effect sensor IC.

The output voltage varies in proportion to the strength of the magnetic field. These devices have low voltage capability, 2.7 Vdc, and are energy efficient with consumption of only 6mA at 5 Vdc. With the low noise output, the external filtering in the integrated circuitry is not required. The sensor ICs can interface with many electrical components without buffering and include firm and thin resistors to allow stability and accuracy at increased temperatures, functioning in a temperature range of -40°C to 100°C. Thus, these devices are highly appropriate for usage in a position detection device.

Based on the theory described in section 3.3.1, two Hall-effect sensors should be mounted half a pole pitch away. Using a 3D printer, a small jig and fixture was designed to ensure the fixed position of two Hall-effect sensors as shown in Figure 3.18. The small fixture positions two Hall-effect sensors at the same height and decreases mounting error. The detailed dimensions of this fixture are presented in Appendix A.

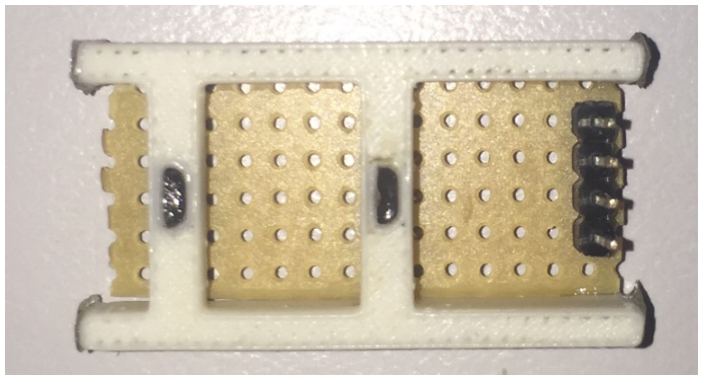

Figure 318: Fixture for Hall-effect sensors.

3.4 Electrical Design of Linear Encoder by Arduino.

3.4.1 Introduction

Section 3.3.1 presented the algorithms for position detection by Hall-effect sensors. The outputs from the Hall-effect sensors are voltage signals, unable to be accepted directly by the servo drivers. Therefore, a microcontroller between the linear Hall-effect sensors and servo driver is needed so that the output of the linear encoder is interpretable by the feedback device of the linear servo driver

Here, the Arduino Board is used to convert the voltage output to a signal from which the servo drivers can read as position feedback. Arduino is an open-source prototyping platform with easy-to-use hardware and simple software [41] allowing it easily to be programmed with Simulink. For this application, the core task of this Arduino board is to transfer the output voltage signal from Hall-effect sensors to the desired differential square wave which can be read by the servo drivers.

3.4.2 Model Design in Simulink.

The Simulink Support Package provides programming blocks for Arduino sensors, actuators, and communication interfaces [42]. In this case, algorithms for the Arduino board were designed based on the algorithm described in 3.3.1 for calculation and signal conversion. The details of the Simulink model are in Appendix B.

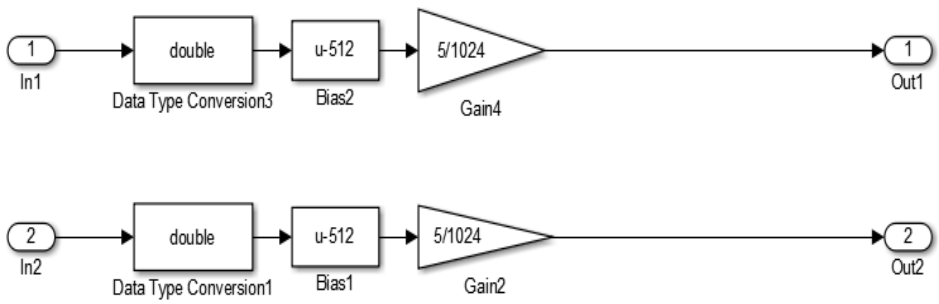

Figure 319: DAC module.

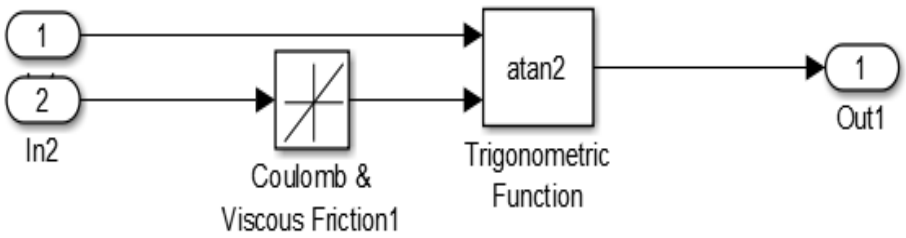

Figure 320: Calculation module

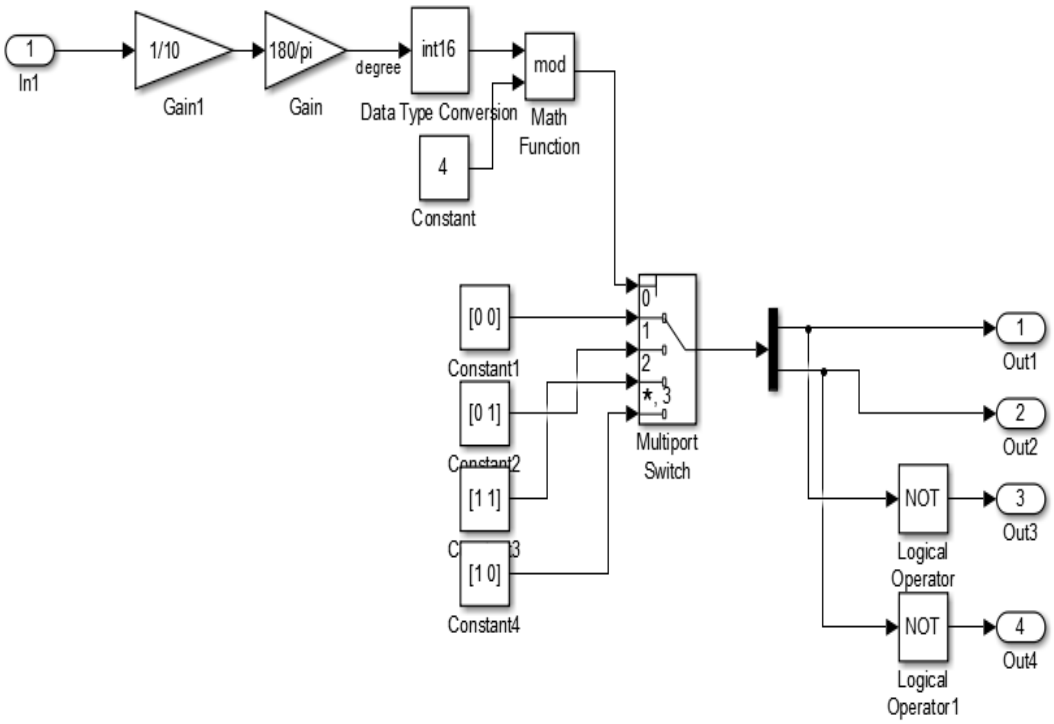

Figure 321: Conversion module.

As shown in Figures 3.19-3.21, the model could be divided into three parts. The purpose of the first part is to convert the digital input value range between 0 and 1023 to a voltage range of 0 to 5 volts. There is a circuit inside the microcontroller that acts as an analog-to-digital converter or ADC to convert the original voltage signal to a digital value. The calculation is performed in the second part of this model, using the trigonometric function block to determine the position. The last part in this model converts the position data to the desired differential square waves.

The first part is a DAC module, the second part is a calculation module and the last part is a conversion module. A Coulomb & Viscous Friction component is used in second part to model Coulomb (static) and viscous (dynamic) friction in case the denominator in trigonometric function comes to '0'. The block models a discontinuity at zero or a linear gain otherwise. The block output matches the algorithm in MATLAB:

where, y is the output, x is the input, Gain is the signal gain for nonzero input values, and offset is the Coulomb friction. With the parameters set as indicated in Figure 3.22, the denominator always has an offset of 0.005 when it approaches zero.

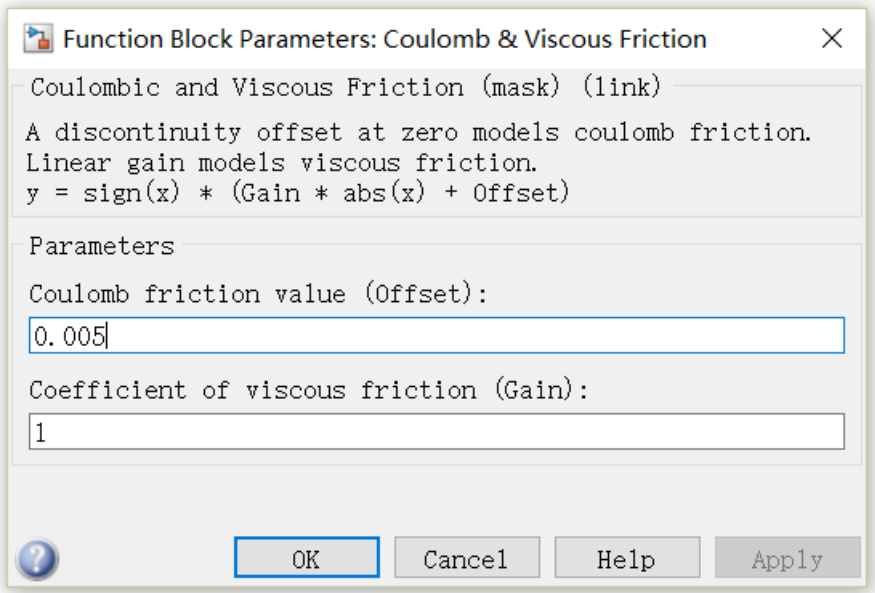

Figure 322: Parameters of the Coulomb & Viscous Friction Block.

In the conversion module, a Data Type block is used to change the data type from 'double' to 'int16'. Next, the signal passes through a Math Function block to determine the reminder after dividing by 4. Finally, a Multiport Switch block is used to obtain the final four digital outputs.

3.5 Conclusions

This chapter described the details of construction for the PMTLM and the linear encoder of Hall-effect sensors. The program design for Arduino in Simulink was also presented. Potential manufacturing problems and solutions were discussed.

The design of the stator should consider the ratio of the length between magnets and steel poles; both the diameter of wire and size of plastic container determine the size of armature and the performance of motor. The simulation of the motor was presented.

The analysis and simulation were presented for the design of linear encoder. It is necessary to pay particular attention to the mounting position of Hall-sensor for

effective performance of the encoder. The plastic fixture was manufactured using a 3D printer.

Finally, the program for Arduino in Simulink was designed. Several important blocks were described in detail allowing the program to run well.

CHAPTER 4 EXPERIMENTAL SETUP

4.1 Introduction

Testing of the PMTLM was performed with a linear servo driver and a servo hydraulic test system. By linking the motor with the position feedback encoder to the linear servo driver, the motor was able to function in an open loop control. The servo hydraulic test system was used to provide thrust output at different currents.

Experimental testing of the position feedback device is also presented in this section.

4.2 Experiments of PMTLM.

A Baldor Microflex brushless AC servo driver [43], which can accept a wide variety of input command signals for specific application needs, was used. This instrument provides simplicity of connection and allows stable performance for the control of both rotary and linear servo motors. The driver is controlled using an external control system. As shown in Figure 4.1, the driver was installed in a safe box with a number of cables exiting the box to allow communication with a PC, 3-phase power, two Input/Output (IO) cards, and encoder.

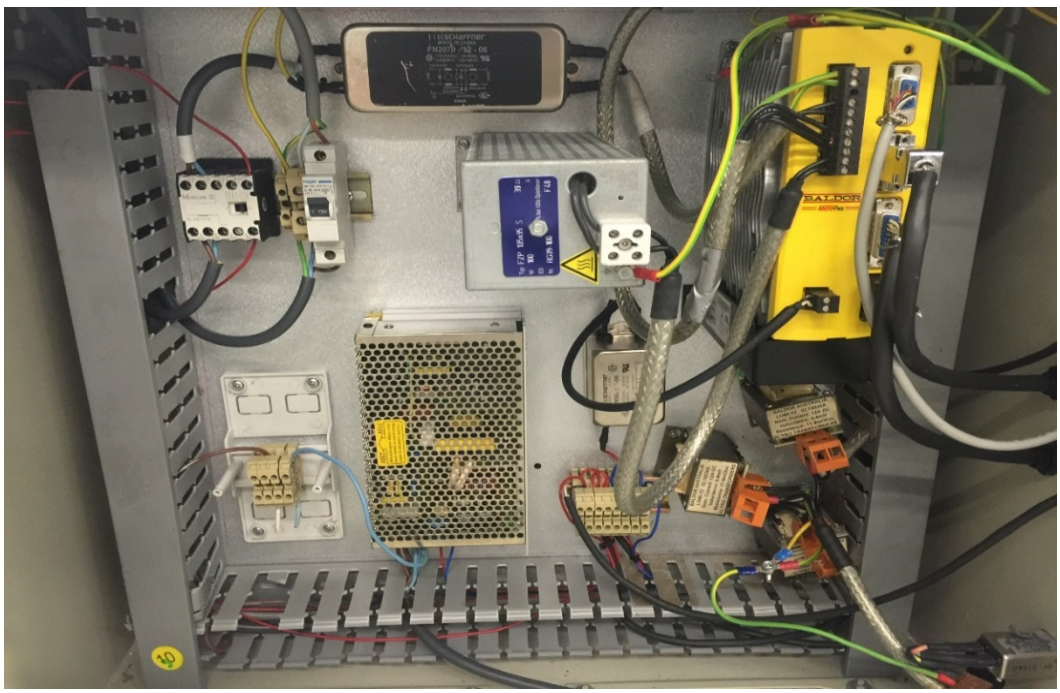

Figure 41: Baldor driver system [24].

In Figure 4.2, the block diagram of the Baldor driver and external control system is illustrated. The Baldor driver was run in current control mode where the current command was generated using an external system developed by Matlab Simulink. This control system allowed regulation of the position and velocity loop and generation of the necessary current.

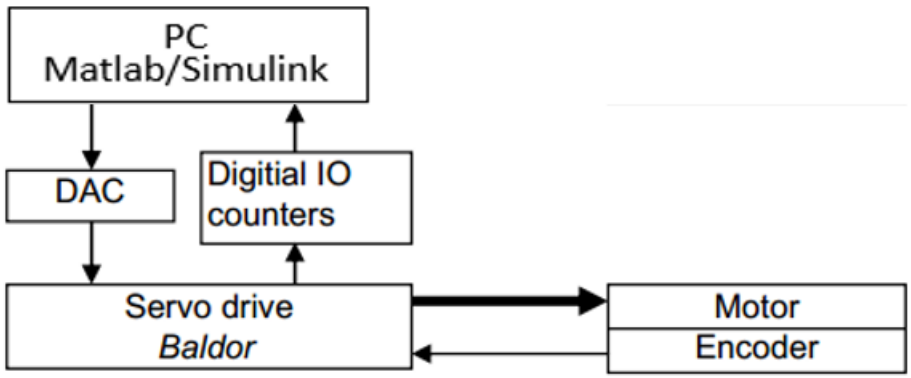

Figure 42: Block diagram of Baldor driver and control system.

The computer had both Matlab and Simulink installed and two mounted IO cards to interface with the Baldor driver. Two National Instrument Cards were used; the analogue IO required a PCI-6024E card and the general digital IO and incremental encoder signals required a PCI-6601 card. These cards were chosen specifically for use with Matlab RTW because the software only supports a limited number of IO cards. The Matlab toolbox Real-Time Workshop (RTW) was used to generate a standalone application that corresponds to the block diagram developed in Simulink.

The servo hydraulic test system is from MTS and is a versatile, high-performance servo hydraulic system for static and dynamic material and component testing.

Two steel fixtures were developed to mount on both sides of the motor as shown in Figure 4.3 which helps maintain the motor in place on the equipment. The upper fixture uses the threaded hole which is also used for the existing flange. Both steel fixtures are detachable. The details of these two fixtures are provided in Appendix A.

The whole system is shown in Figure 4.3.

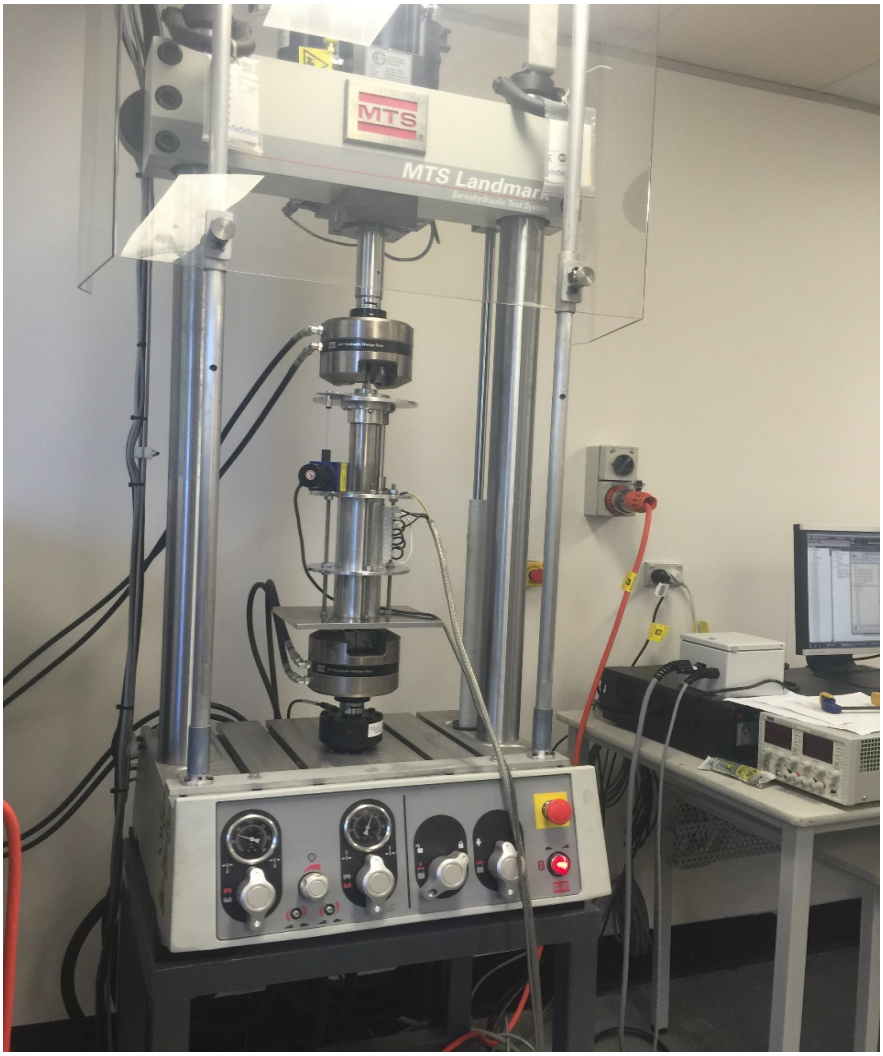

Figure 43: Thrust measurement system.

4.3 Experimental Testing the Position Feedback Device.

The position feedback device is mounted on the PMTLM with the high precision rope encoder feedback system. The block diagram of this experiment is shown in Figure 4.4. The National Instruments (NI) PCI board was used as the control board connecting Matlab and the motor using a Simulink desktop real-time control model. This platform enables Matlab/Simulink to simulate and control the system in real-time. The A/D and D/A driver blocks were from the National Instruments Simulink library.

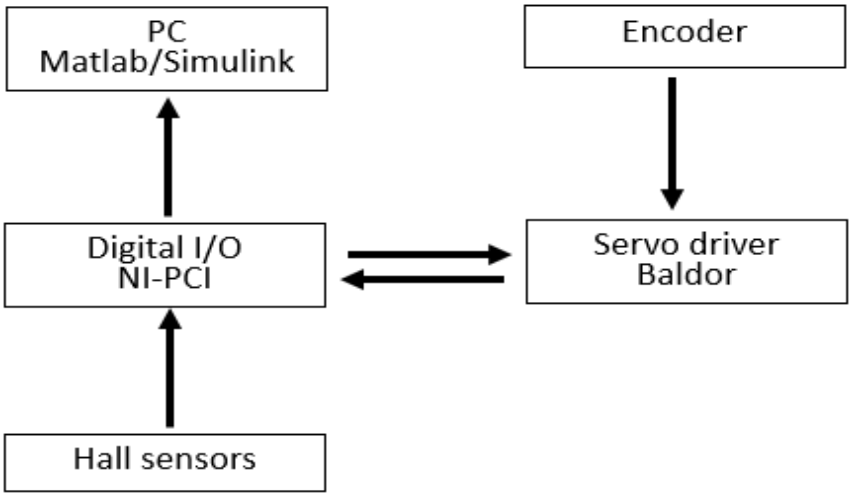

Figure 44: Block diagram of Hall sensor experiment.

The Hall sensors were mounted at three positions which are 3mm, 5mm, or 7mm away from the tube with the permanent magnets. Then, the measured data transferred to the Matlab by NI-PCI board. The final results can be calculated in the Matlab.

4.4 Conclusions

This chapter presents all the experimental equipment for both the PMTLM thrust test and Hall position feedback device. The MTS servo hydraulic test system is the core part of the thrust test; the designed motor was connected with a Baldor driver so that with different input currents, the output force could be measured. The Hall position feedback device was mounted on a mature linear motor test-bed, with a high precision rope encoder as reference.

CHAPTER 5 RESULTS

5.1 Introduction

This chapter analyses the thrust output results for the PMTLM. The FEA model simulation results are presented as a benchmark for actual experimental results collected by MTS servo hydraulic test system. The experimental data validate the simulation results. By applying different currents, the relationship between output force and current could be determined.

The output voltages from the Hall sensors were collected via NI PCI board and analysed using Matlab. This chapter compares the error for the three positions and determines the ideal mounting position for the device.

5.2 Force Generation

Determining the force output of the motor in an indirect way, such as based on the motor current, can be useful. Since the relationship between force output and current is nearly linear for a PM motor, the motor currents can be used to determine the amount of force that is generated easily.

5.2.1 Simulated Force Output

The force output of the drive was simulated using Flux 2D FEA software. A 2D axisymmetric model of the magnetic stator and the coils was developed. As described in section 3.2.3, the circuit consisted of 12 coils in three-phase power with rated current 3A and peak current 10A.

The model was simulated keeping the armature in a fixed location and running a whole electrical cycle through the coils. The current was stepped from 0A to 3A in 0.3A increments to create a map of generated force output as shown in Figure 5.1. The X-axis is the electrical angle and the Y-axis is the simulated force output.

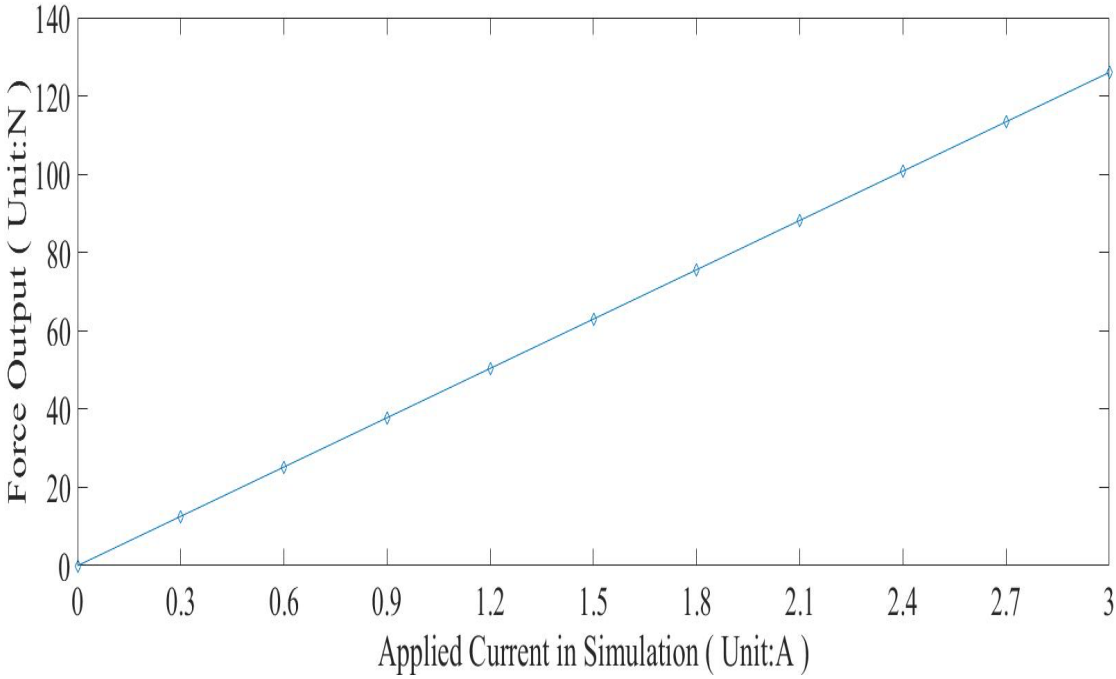

Figure 51: Simulated force output.

5.2.2 Experimental Force Output

The experimental method for determining the force constant of the motor is to apply different input currents while the motor is held stationary. The MTS servo hydraulic test system then measured the output force when the motor is running.

Figure 5.2 shows the output force of the motor as a function of the input current applied to the motor. The applied current is from 0A to 3A, which is the rated current of the motor, with 10% increment. The motor exhibits a linear relationship between the force and the current as predicted from simulation. For a given current, the motor's constant force can be calculated and can be used as an indirect method to get the force output.

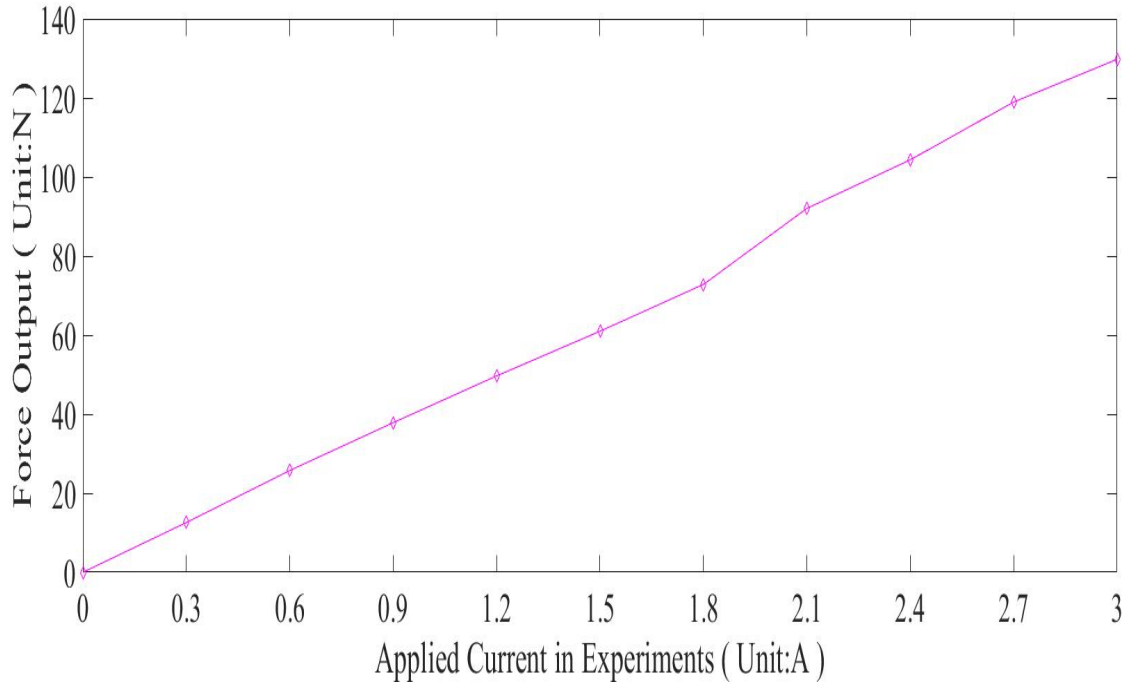

Figure 52: Measured motor force as a function of applied current.

Table 51: Measurement of force at different applied current.

Applied Current (A)	Output Force (N)	Force constant (N/A)
0.3	12.58	41.93
0.6	25.74	42.90
0.9	37.85	42.06
1.2	49.67	41.39
1.5	60.98	40.65
1.8	72.82	40.46
2.1	92.05	43.83
2.4	104.34	43.48
2.7	118.97	44.06
3.0	129.77	43.26

Table 5.1 presents the measured output force of the applied current. The results ranged from 40N/A to 44N/A. Some of this variation may be due to the residual current and also to the manufacturing process when using small current. The relatively fixed force constant suggests that the PMTLM designed here is a reliable product.

5.3 Hall Position Feedback Device

The results analysed the magnetic field data in three positions above the PM stator. Both the simulation and experimental results are presented in this section.

5.3.1 Magnetic Field Distribution in Simulation

To determine the ideal position, the magnetic flux distributions at 3mm, 5mm and 7mm away from the stator were examined. As shown in Figures 5.3, when the path was 7mm away from the stator, the magnetic flux distribution looks more sinusoidal than the distribution on the path of 3mm and 5mm. However, the magnetic field strength is lowest in 7mm.

Figure 53: Magnetic flux distribution.

In Figure 5.4 to Figure 5.5, the harmonic analyses in these three positions along X and Y component are presented respectively. First of all, there is no big difference between two directions. As a result, the experiment could just pick one direction. Secondly, the harmonic analysis result shows the magnetic flux distribution is more sinusoidal in 7mm.

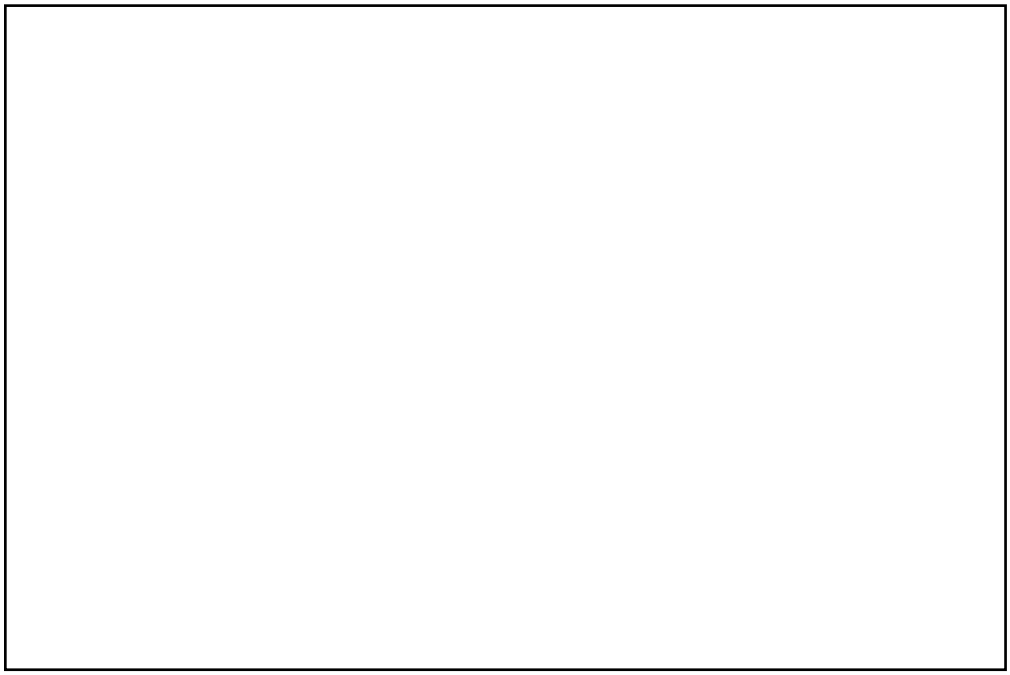

Figure 54: Harmonic analysis along X component.

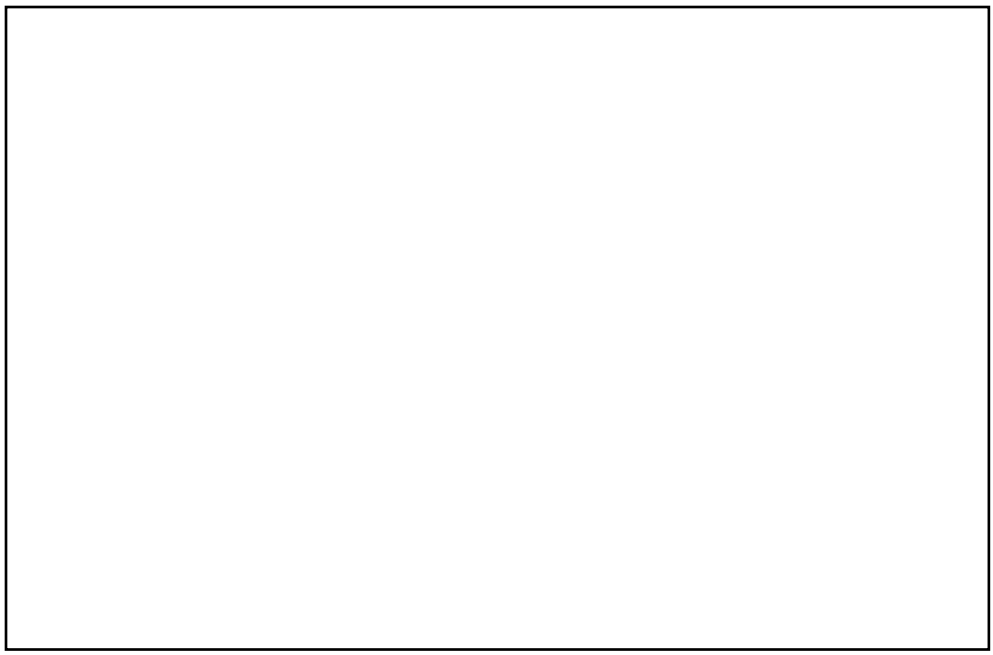

Figure 55: Harmonic analysis along Y component.

5.3.2 Experimental Results

The output voltage of Hall sensors in three different positions were collected by NI-PCI board. The measured flux signal was used to calculate the position of the motor

according to the algorithm in section 3.3.2. This calculated position was compared to the position given by the high accuracy encoder. The error between the encoder position and the Hall sensor position are shown in Figure 5.6 to Figure 5.8 for 3, 5, or 7mm positioning.

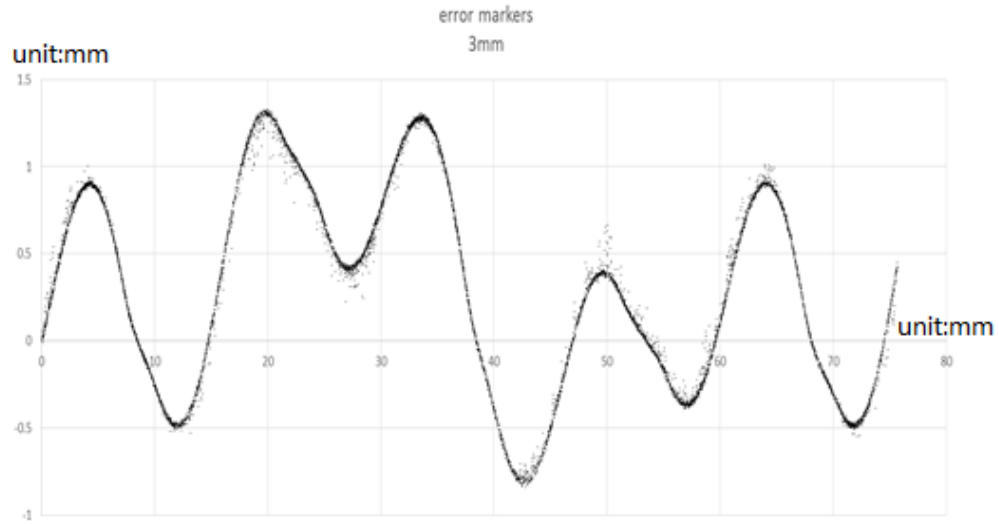

Figure 56: Distribution of error markers (3mm).

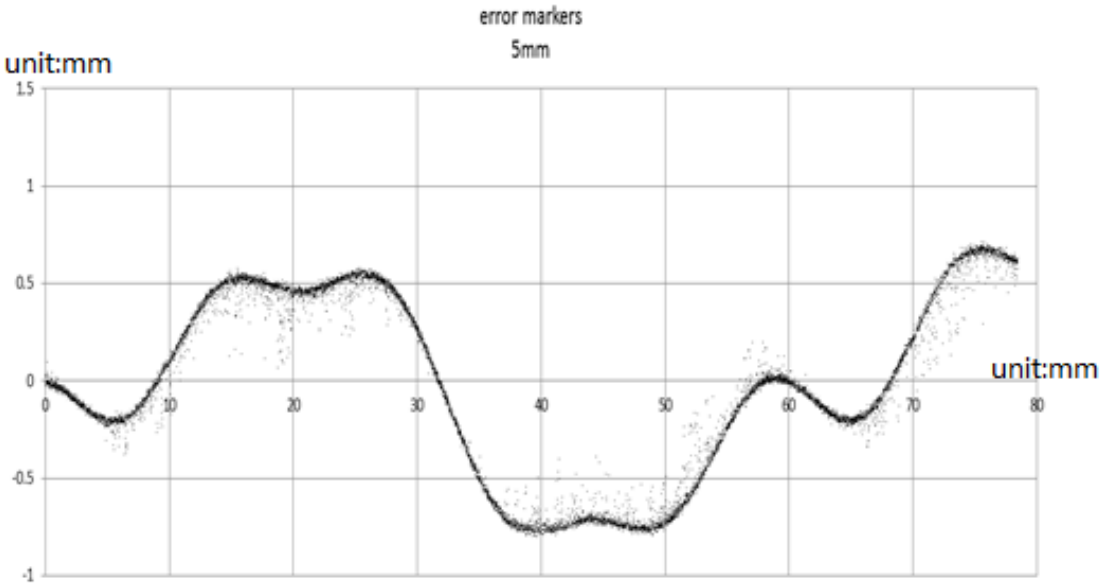

Figure 57: Distribution of error markers (5mm).

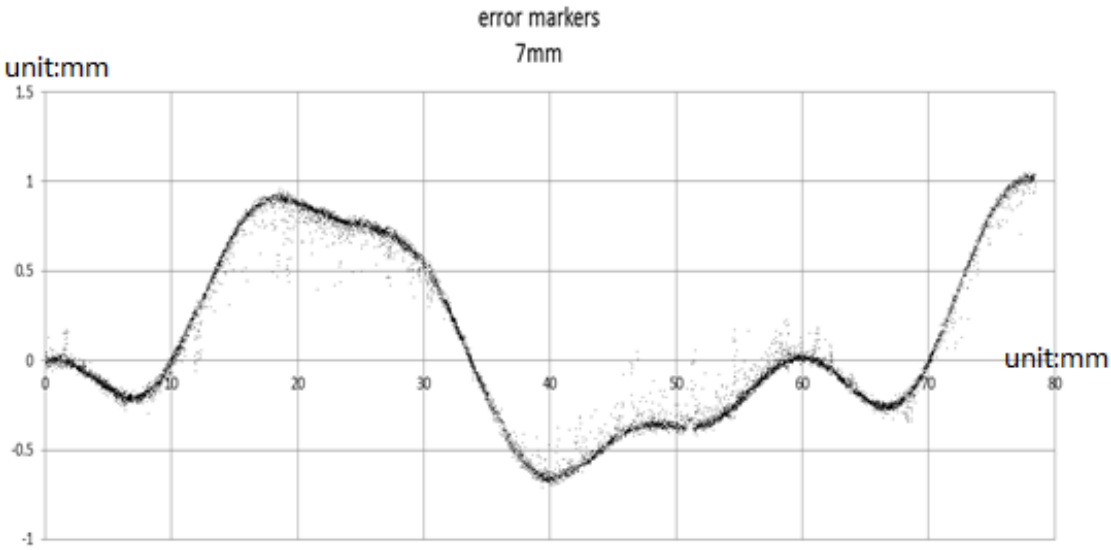

Figure 58: Distribution of error markers (7mm).

The experimental observation shows that the measurement error is lowest when the Hall sensor is 5mm away from the stator. Though the magnetic flux distribution at 7mm is more sinusoidal than that at 5mm, the output results are more accurate when the Hall sensors are 5mm away from the stator because the output is calculated by a

trigonometric function which is influenced by the strength of the magnetic flux as well as by the sinusoidal nature of the magnetic flux distribution.

More specifically, when the Hall sensor ICs are mounted at 7mm, the magnetic flux strength decreases, which would affect the final results greatly. As a result, the ideal mounting position in this case for Hall sensor ICs is 5mm away from the stator.

5.4 Conclusion

This chapter analysed the force output of PMTLM and the appropriate mounting position for Hall sensor ICs.

Ten currents with 10% increment to the rated current 3A were applied to the PMTLM and the homologous force output was collected. These data allowed calculation of the force constant of this motor.

By comparison of the data collected from the Hall sensor ICs mounted in three different positions, the optimal mounting position was selected.

CHAPTER 6 CONCLUSIONS AND RECOMMENDATIONS

6.1 Summary

The aim of this thesis is to develop a device with strong output force and limited size which could be used as the vehicle vibration reduction device. A complete design of Permanent Magnet Tubular Linear Motor was presented and a corresponding position feedback device based on Hall sensor ICs was developed as well.

Although there were several problems coming out during the project, the design and manufacturing were completed along with basic tests.

6.2 PMTLM

The Permanent Magnet Tubular Linear Motor was fully designed and manufactured in my project. The PMTLM was connected to a standard servo driver and basic testing completed by this servo driver.

The performance of PMTLM designed here may not outstanding, especially comparing with some industrial grade products, however, the motor force constant of this motor is 42.4N/A which is still higher than the PMTLM mentioned in [24]. It is mainly due to the size of permanent magnets and the coil winding method. This PMTLM could be used in many applications such as vehicle damping system.

The MTS servo hydraulic test system is the core part of the thrust test; the designed motor was connected with a Baldor driver so that with different input currents, the output force could be measured. With the reliable force constant, this motor could be used in many further applications with a servo driver.

6.3 Position Feedback Device

In this work, a Hall-effect sensor position detection method for tubular linear motor is proposed. The FEA model is developed to simulate the magnetic flux density of tubular linear motor. Considering minimizing the error of measurements, a high precision rope encoder feedback was used. The advantage of the proposed Hall-effect sensor detection system is its lower cost, simple and convenient with satisfactory accuracy. By comparing the different positions of Hall sensor, and

choosing the suitable algorithm to calculate the results, the higher precision and lower cost solution of position detection has been found. The Hall-effect sensor position detection is suitable for most low-cost tubular linear motor systems.

6.4 Recommendations for Future Work

In the future, there are still more areas of interest that can be explored about the PMTLM. For example, by applying the fixed current to the PMTLM, how the output force would change with the different armature positions. Moreover, different number of Hall sensor ICs could be used in the future research rather than two. The relationship between the magnet size and magnetic flux distribution also could be researched in the future.

REFERENCES

[1] R. E. C. D. Howe, and A. Q. Zhu, "Status of linear drive technologies in europe," 2001.

[2] E. R. Laithwaite, "A History of Linear Electric Motors," 1987.

[3] E. R. Laithwaite, *Exciting electrical machines*: Pergamon, 1974.

[4] R. Hellinger and P. Mnich, *Linear Motor-Powered Transportation: History, Present Status, and Future Outlook*.

[5] J. F. Gieras, Z. J. Piech, and B. Tomczuk, *Linear synchronous motors: transportation and automation systems*: CRC press, 2011.

[6] N. Corsi, R. Coleman, and D. Piaget, "Status and new development of linear drives and subsystems," in *6th International Symposium on Linear Drives for Industry Applications (LDIA2007), Conference Publication, Lille*, 2007, pp. 16-19.

[7] Y. Suzuki and H. Nakamata, "Linear motor structure," ed: Google Patents, 2000.

[8] J. Wang, D. Howe, and Z. Lin, "Comparative Studies on Linear Motor Topologies for Reciprocating Vapor Compressors," in *2007 IEEE International Electric Machines & Drives Conference*, 2007, pp. 364-369.

[9] J. Wang and G. W. Jewell, "A General Framework for the Analysis and Design of Tubular Linear Permanent Magnet Machines," *IEEE Transactions on Magnetics,* vol. 35, p. 1986, 1999.

[10] G. Otten, T. J. De Vries, J. Van Amerongen, A. M. Rankers, and E. W. Gaal, "Linear motor motion control using a learning feedforward controller," *Mechatronics, IEEE/ASME Transactions on,* vol. 2, pp. 179-187, 1997.

[11] P. Hor, Z. Zhu, D. Howe, and J. Rees-Jones, "Minimization of cogging force in a linear permanent magnet motor," *Magnetics, IEEE Transactions on,* vol. 34, pp. 3544-3547, 1998.

[12] A. Chitayat, "Flat linear motor," ed: Google Patents, 1998.

[13] Z. Q. Z. P. J. Hor, and D. Howe, "Eddy current loss in a moving-coil tubular permanent magnet motor," *Magnetics, IEEE Transactions on,* vol. 35, 1999.

[14] W.-M. Zhang, "Linear motor compressor," ed: Google Patents, 2001.

[15] S. B. N. Bianchi, and J. Corda, "Tubluar linear motors: A comparison of brushless PM and SR motors," *Power Electronics, Machines and Drives, 2002. International Conference on (Conf. Publ. No. 487),,* vol. 1, pp. 626-631,

2002.

[16] S. B. N. Bianchi, D. D. Corte, and F. Tonel, "Tubular linear permanent magnet motors: An overall comparison," *Industry Applications, IEEE Transactions,* vol. 39, pp. 466-475, 2003.

[17] X. Liu, Y. Ye, Z. Zheng, and Q. Lu, "A novel tubular permanent magnet linear synchronous motor used for elevator door," in *Electrical Machines and Systems, 2007. ICEMS. International Conference on*, 2007, pp. 801-804.

[18] A. W. J. Hsue, M. T. Yan, and S. H. Ke, "Comparison on linear synchronous motors and conventional rotary motors driven Wire-EDM processes," *Journal of Materials Processing Technology,* vol. 192–193, pp. 478-485, 10/1/ 2007.

[19] K. Jiwon, L. Jiyoung, K. Dohyun, K. Kwangwoon, and C. Junghwan, "Linear position detection method using magnetic sensors for transverse flux linear motor," in *Electromagnetic Field Computation (CEFC), 2010 14th Biennial IEEE Conference on*, 2010, pp. 1-1.

[20] C. H. Chen and M. Y. Cheng, "Design and implementation of a cost-effective position control system for an ironless linear motor," *IEE Proceedings – Electric Power Applications,* vol. 152, pp. 1223-1232, 2005.

[21] L. Xiao, X. Liu, Y. Ye, and Z. Zheng, "Study of the linear Hall-effect sensors mounting position for PMLSM," ed, 2007, pp. 1175-1178.

[22] S. Paul and C. Junghwan, "A New Approach to Detect Mover Position in Linear Motors Using Magnetic Sensors," *Sensors (14248220),* vol. 15, pp. 26694-26708, 2015.

[23] "www.copleycontrols.com," *Copley Controls Corporation,* Sept 2010.

[24] P. A. Commins, " Development and analysis of two alternative tubular linear motors for use in machine tools," Doctor of Philosophy thesis, School of Mechanical, Materials and Mechatronic Engineering, University of Wollongong, 2013.

[25] X. Yanliang and L. Xiquan, "Development of Tubular Linear Permanent Magnet Synchronous Motor Used in Oil-well Field," *Telkomnika,* vol. 9, pp. 515-522, 2011.

[26] K. Li, X. Zhang, and H. Chen, "Design Optimization of a Tubular Permanent Magnet Machine for Cryocoolers," *IEEE Transactions on Magnetics,* vol. 51, pp. 1-8, 2015.

[27] J. Wang, D. Howe, and G. W. Jewell, "Analysis and Design Optimization of an Improved Axially Magnetized Tubular Permanent-Magnet Machine," *IEEE Transactions on Energy Conversion,* vol. 19, pp. 289-295, 2004.

[28] N. Bianchi, "Analytical field computation of a tubular permanent-magnet linear motor," *Magnetics, IEEE Transactions on,* vol. 36, pp. 3798-3801, 2000.

[29] B. Tomczuk, G. Schröder, and A. Waindok, "Finite-element analysis of the magnetic field and electromechanical parameters calculation for a slotted permanent-magnet tubular linear motor," *Magnetics, IEEE Transactions on,* vol. 43, pp. 3229-3236, 2007.

[30] G. M. J. Atencia, A. García Rico, and J. Flórez, "Minimization of cogging force in flat permanent magnet linear drives," *The Third International Symposium on Linear Drives for Industrial Applications,* 2001.

[31] A. Van Zyl and C. Landy, "Reduction of cogging forces in a tubular linear synchronous motor by optimising the secondary design," in *Africon Conference in Africa, 2002. IEEE AFRICON. 6th*, 2002, pp. 689-692.

[32] Y. M. M. Ohto, and Y. Tsutsui, "Linear motor's cogging minimization using quality engineering and finite element method," 2005.

[33] N. Bianchi, S. Bolognani, D. D. a. Corte, and F. Tonel, "Tubular linear permanent magnet motors: an overall comparison," *Industry Applications, IEEE Transactions on,* vol. 39, pp. 466-475, 2003.

[34] W. Jiabin, G. W. Jewell, and D. Howe, "A general framework for the analysis and design of tubular linear permanent magnet machines," *Magnetics, IEEE Transactions on,* vol. 35, pp. 1986-2000, 1999.

[35] G. Remy, J. Gomand, T. Abdelmounaïm, and B. Pierre-Jean, "Analysis of the force ripples of a current loaded PMLSM," *Compel,* vol. 28, pp. 750-761, 2009

2014-05-21 2009.

[36] Y. Liang, H. Jie, J. Zongxia, I. M. Chen, and L. Chee Kian, "Flux distribution and back-iron influence of tubular linear motors," in *Fluid Power and Mechatronics (FPM), 2011 International Conference on*, 2011, pp. 1-6.

[37] N. Bianchi, S. Bolognani, and J. Corda, "Tubular linear motors: A comparison of brushless PM and SR motors," *IEE conference publication,* pp. 626-631, 01/01 2002.

[38] N. Bianchi, S. Bolognani, D. D. Corte, and F. Tonel, "Tubular linear permanent magnet motors: an overall comparison," *Industry Applications, IEEE Transactions on,* vol. 39, pp. 466-475, 2003.

[39] J. F. Eastham, R. Akmese, and H. C. Lai, "Optimum design of brushless tubular linear machines," *Magnetics, IEEE Transactions on,* vol. 26, pp. 2547-2549, 1990.

[40] G. Thangavel, D. Chatterjee, and A. K. Ganguli, "FEA Simulation Models based Development and Control of An Axial Flux PMLOM," *International Journal of Modelling and Simulation of Systems,* vol. 1, pp. 74-80, 2010.

[41] "https://www.arduino.cc/en/Guide/Introduction," *Arduino,* 2013.

[42] "http://au.mathworks.com/hardware-support/arduino-

simulink.html?requestedDomain=www.mathworks.com#," *Mathworks,* 2014.

[43] "www.baldor.com.au," *Baldor,* May 2011.

APPENDIX A: MOTOR DETAILS

This appendix contains the details of parts of designed motor throughout this research. Detailed drawings of the entire components manufactured in workshop are provided.

Figure A.1 shows the complete assembly manufactured in workshop in University of Wollongong. The additional linear rope encoder and linear bearing were purchased in the market to fit this motor.

The drawings of each component are presented in the following pages.

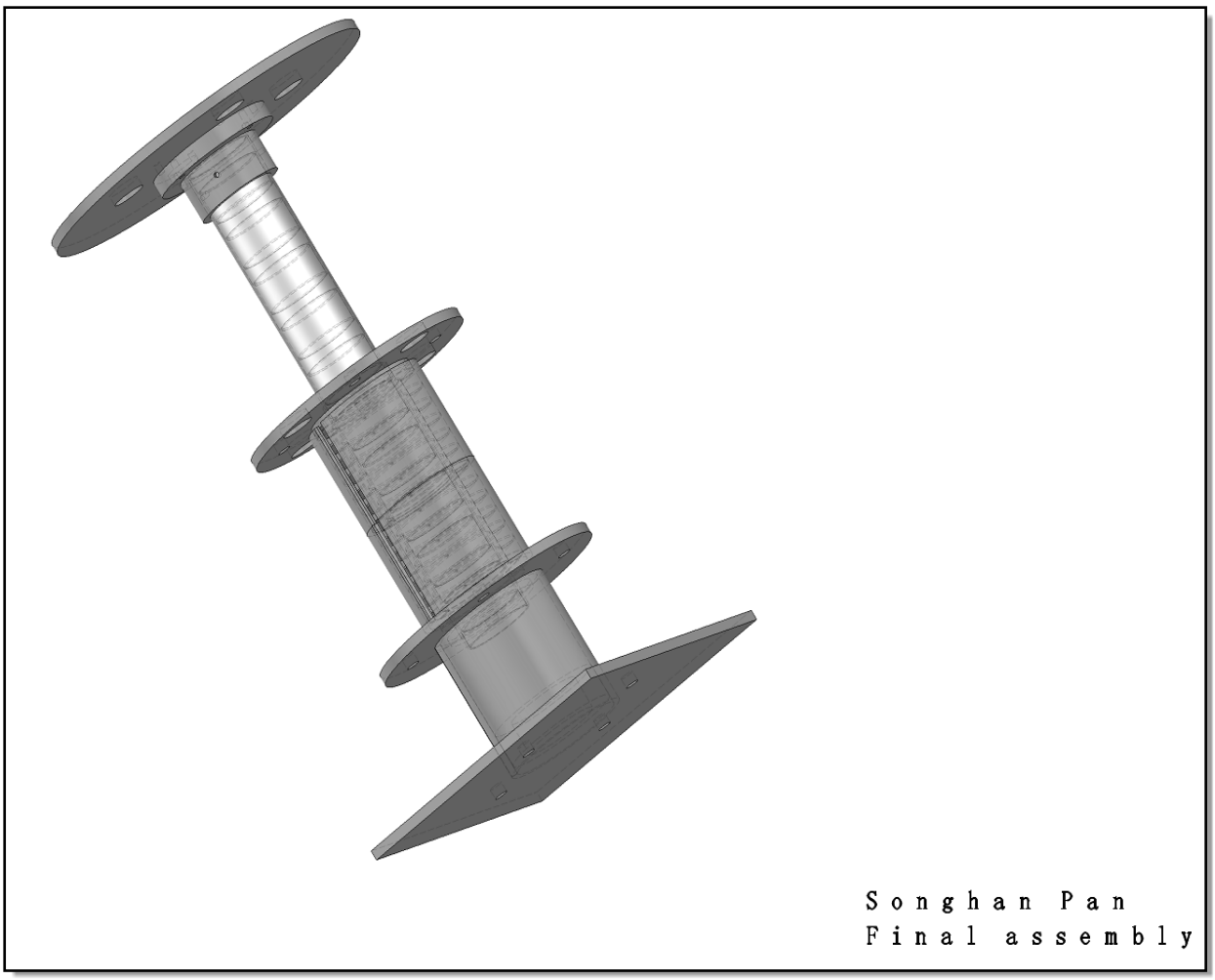

Figure A1: Complete Assembly

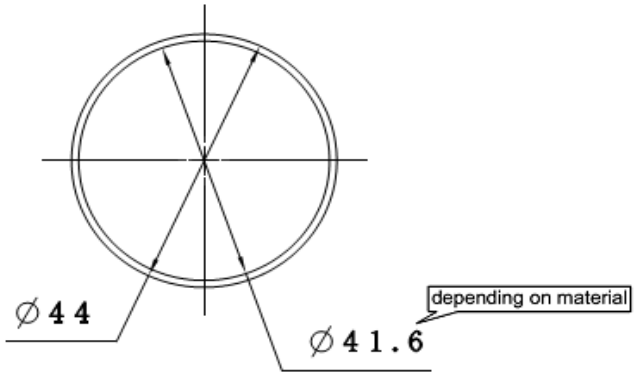

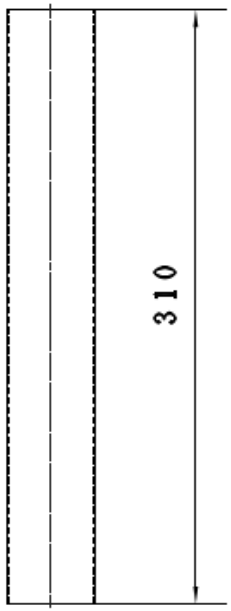

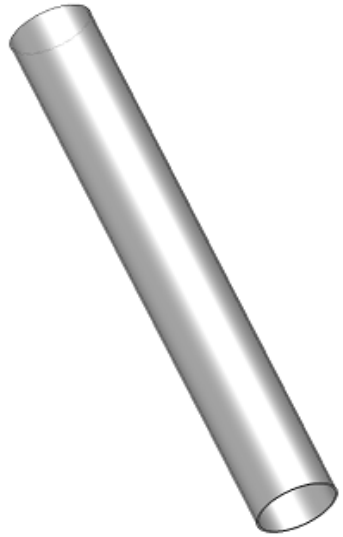

Songhan Pan
stainless steel tube
Quantity:1

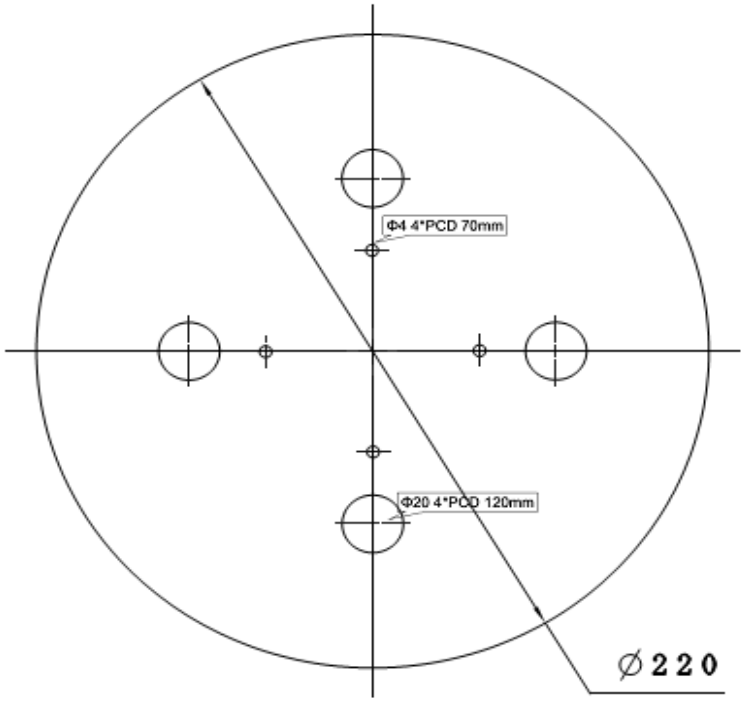

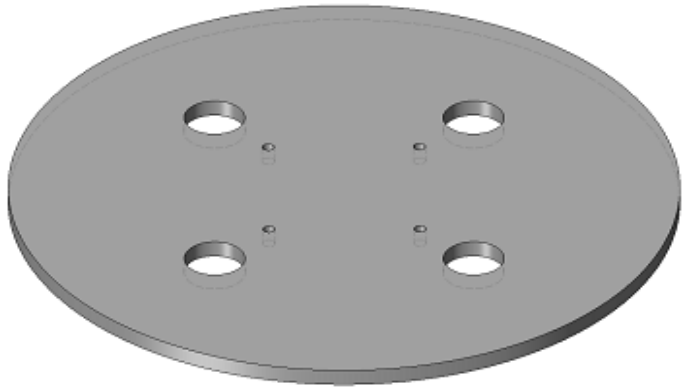

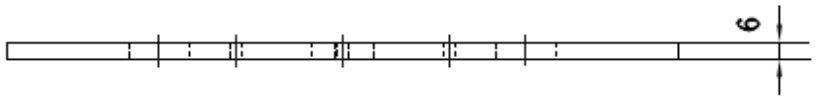

Songhan Pan
Top cap
Quantity: 1
Material: Aluminum

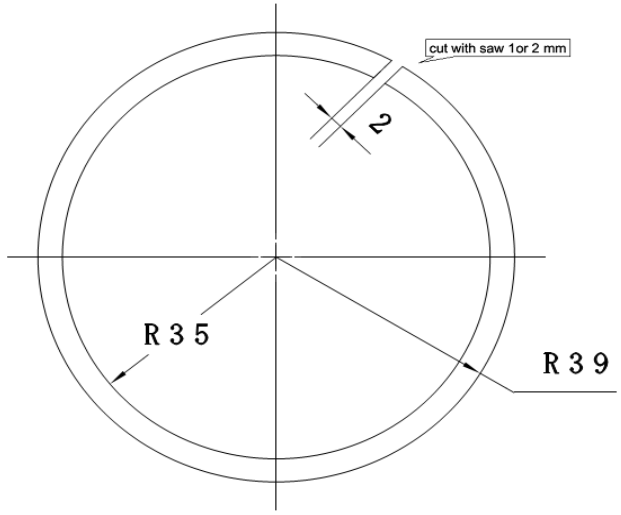

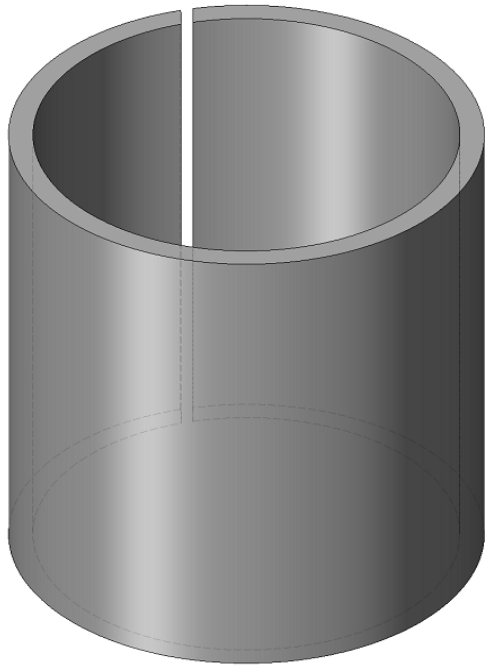

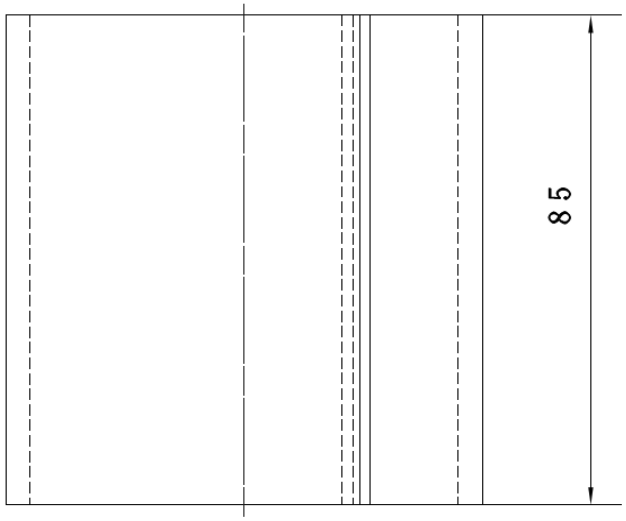

Songhan Pan
Material: Aluminum
quantity:1

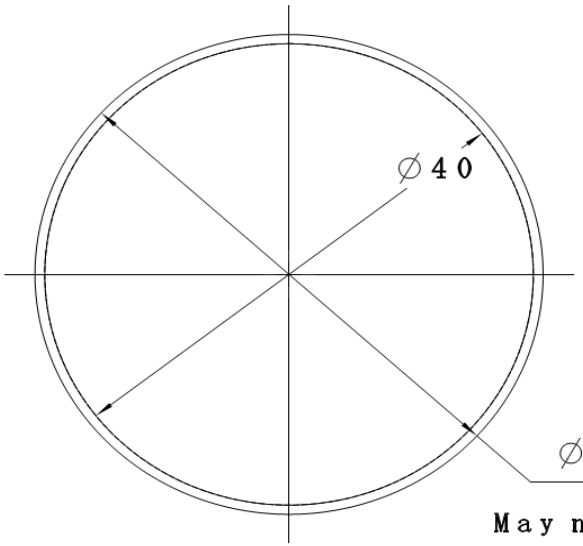

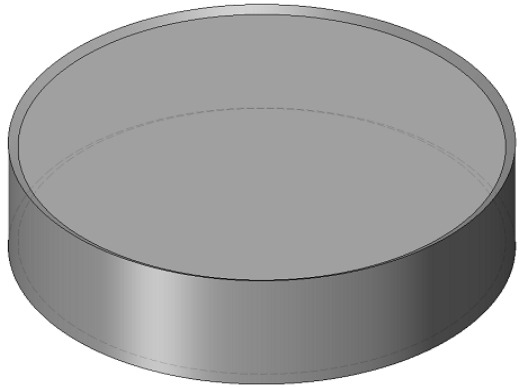

May need adjust when material arrives.

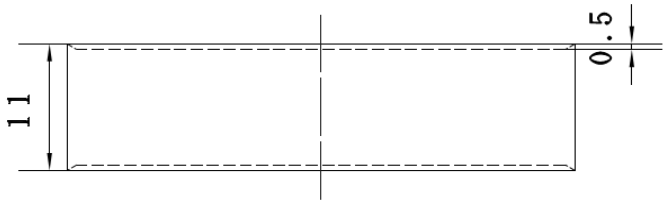

steel
oiled dipped. to stop rust.

Songhan Pan
steel pole shoes
Quantity:11

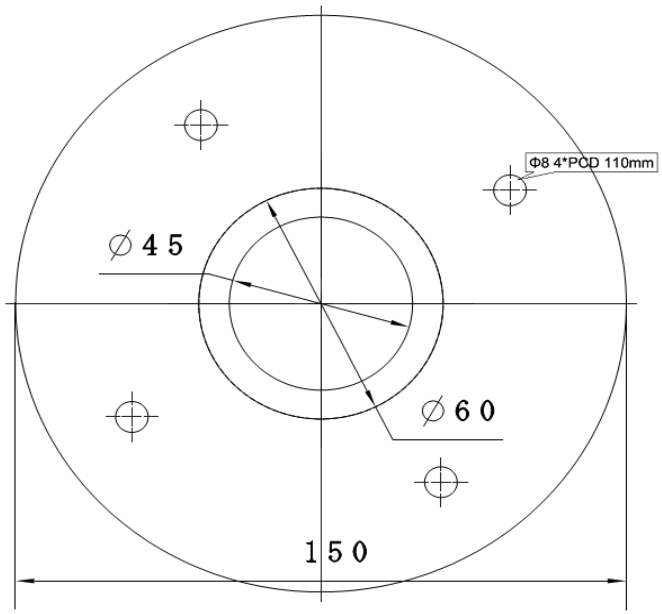

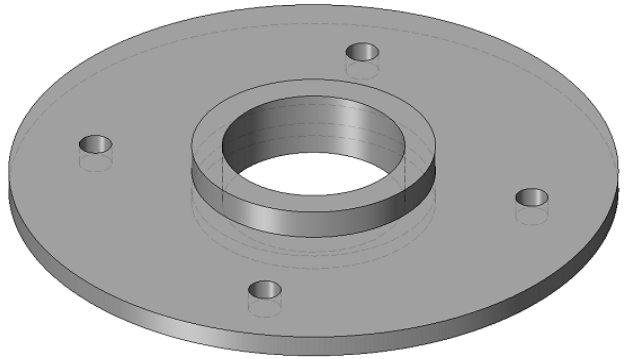

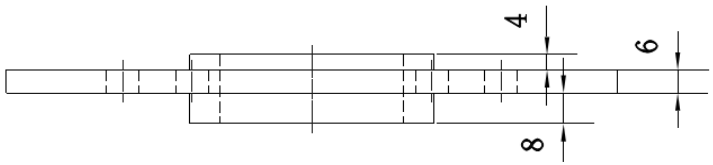

Songhan Pan
mid cap 2
Material: Aluminum
Quantity:1

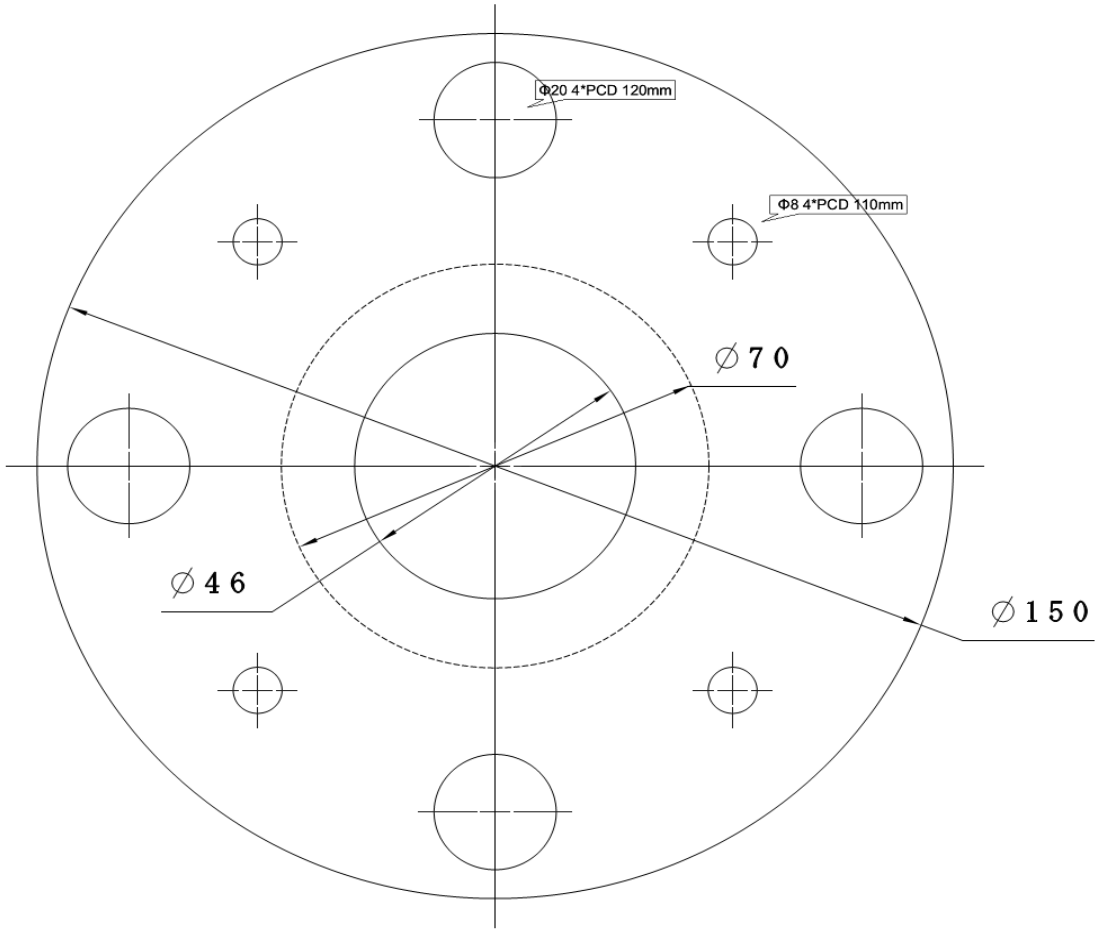

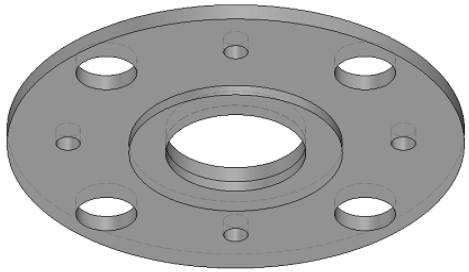

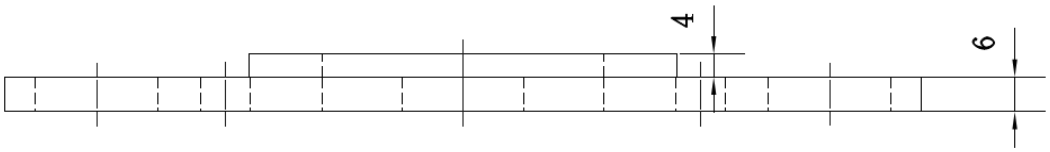

Songhan Pan
mid cap 1
Material: Aluminum
Quantity: 1

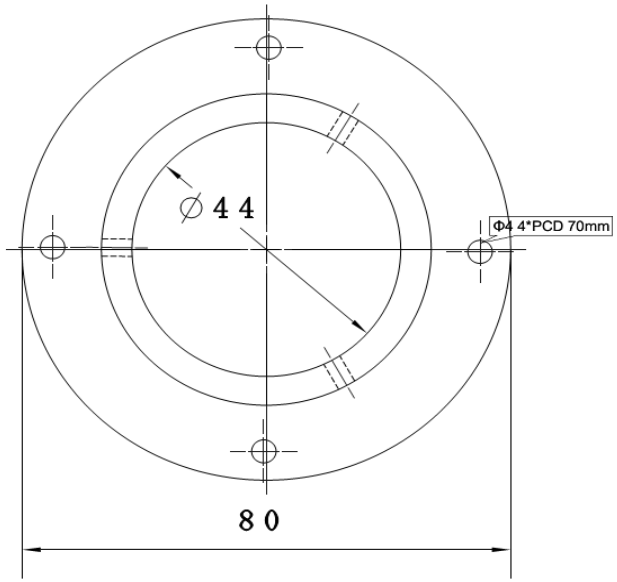

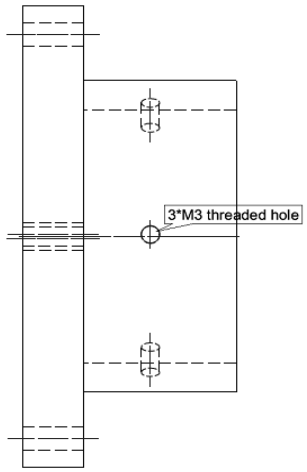

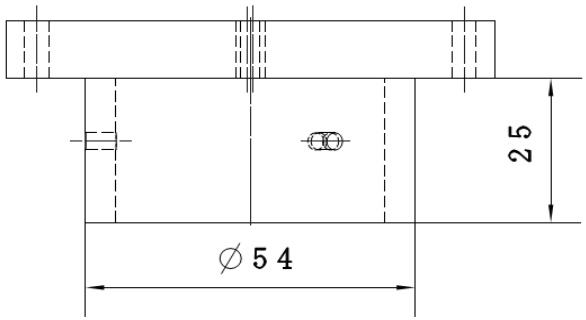

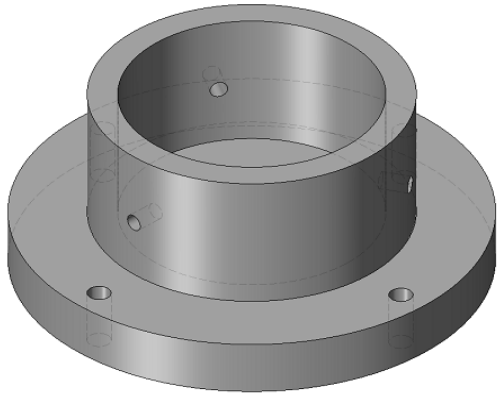

Songhan Pan
Flange
Material: Aluminum
Quantity: 1

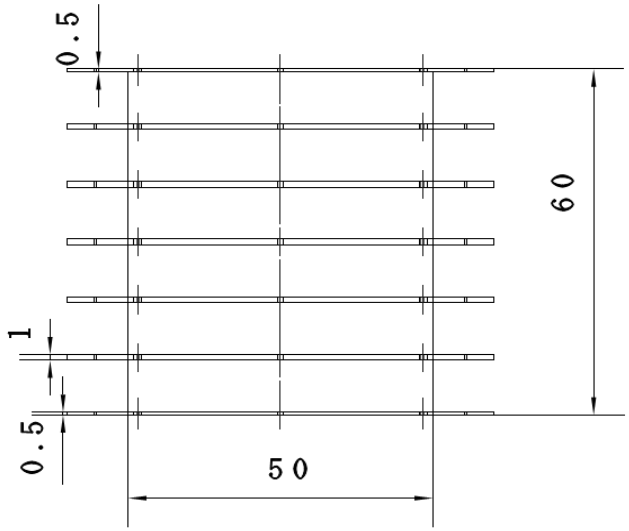

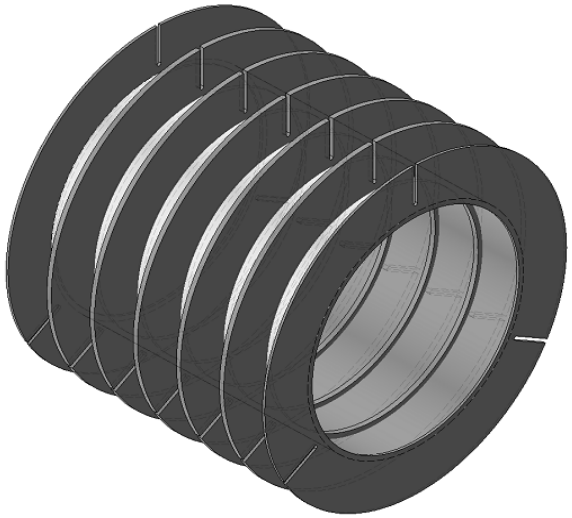

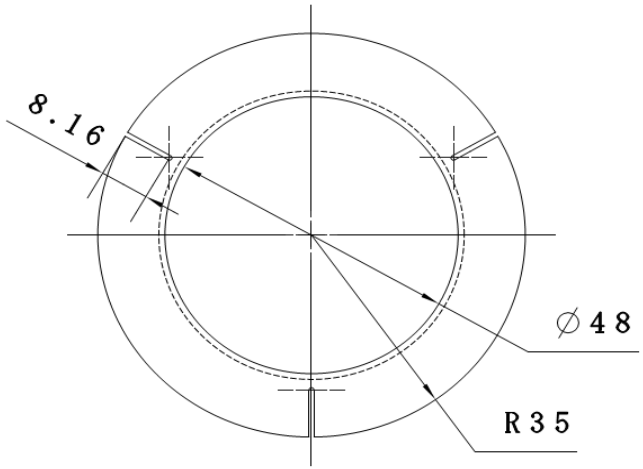

Songhan Pan
coils container
Material: Plastic
Quantity: 2

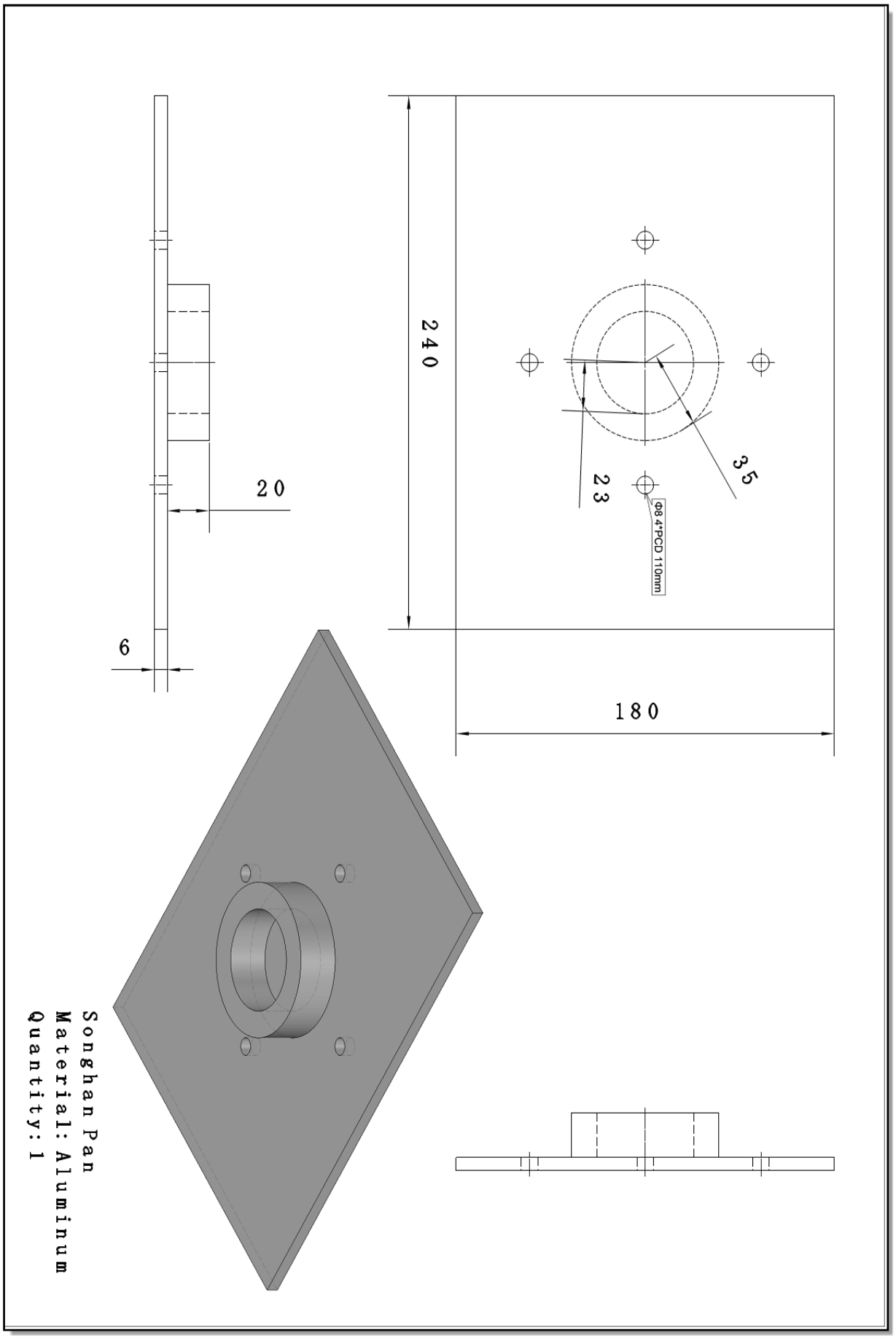
240
180
20
6
23
35
Φ8 4*PCD 110mm
Songhan Pan
Material: Aluminum
Quantity: 1

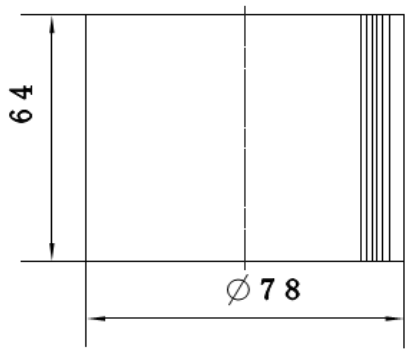

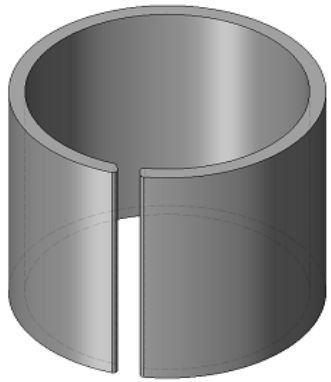

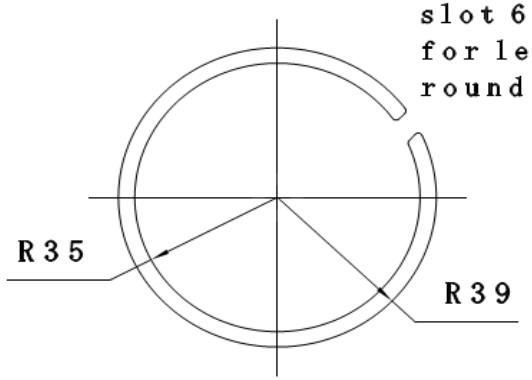

slot 6mm cut
for letting cables out.
round corners so sharp edge is gone.

Songhan Pan
Quantity:2
Material: Aluminum
Name of part: Back plate

APPENDIX B: SIMULATINK MODEL